

# Dynamic Modeling of Branched Robots using Modular Composition

Frederico Fernandes Afonso Silva and Bruno Vilhena Adorno

**Abstract**—When modeling complex robot systems such as branched robots, whose kinematic structures are a tree, current techniques often require modeling the whole structure from scratch, even when partial models for the branches are available. This paper proposes a systematic modular procedure for the dynamic modeling of branched robots comprising several subsystems, each composed of an arbitrary number of rigid bodies, providing the final dynamic model by reusing previous models of each branch. Unlike previous approaches, the proposed strategy is applicable even if some subsystems are regarded as black boxes, requiring only twists and their time derivatives, and wrenches at the connection points between those subsystems. To help in the model composition, we also propose a weighted directed graph representation where the weights encode the propagation of twists and their time derivatives, and wrenches between the subsystems. A simple linear operation on the graph interconnection matrix provides the dynamics of the whole system. Numerical results using a 24-DoF fixed-base branched robot composed of eight subsystems show that the proposed formalism is as accurate as a state-of-the-art library for robotic dynamic modeling. Additional results using a 30-DoF holonomic branched mobile manipulator composed of three subsystems demonstrate the fidelity of our model to a modern robotics simulator and its capability of dealing with black box subsystems. To further illustrate how the derived dynamic model can be used in closed-loop control, we also present a simple formulation of a model-based wrench-driven pose control for branched robots.

**Index Terms**—Branched robots, Modular dynamic modeling, Newton-Euler formalism, Topological graph, Model-based control.

## I. INTRODUCTION

In the robotics literature, the Newton-Euler formalism is usually presented at the level of each rigid body in the mechanical structure, notably by analyzing the effects of twists and wrenches at the  $i$ th link/joint/CoM. This provides a systematic dynamic modeling strategy applicable to serial manipulators [1], [2] and open kinematic trees [3], [4], [5]. However, approaches based on this formalism typically give a monolithic solution to the system and do not allow model composition. See, for instance, the formulations presented in [6].

F. F. A. Silva and B. V. Adorno are with the Department of Electrical and Electronic Engineering and the Manchester Centre for Robotics and AI, The University of Manchester, Oxford Road, Engineering Building A, Manchester M13 9PL, United Kingdom (emails: frederico.silva@ieee.org; bruno.adorno@manchester.ac.uk).

This work was partly done when the authors were affiliated with the Federal University of Minas Gerais, Belo Horizonte, MG, Brazil, and supported by the Brazilian agency CAPES, the UK Research and Innovation (UKRI) under the UK government's Horizon Europe funding guarantee [grant number EP/Y024508/1], and the Royal Academy of Engineering under the Research Chairs and Senior Research Fellowships programme.

## NOMENCLATURE

$s$	Number of subsystems of the branched robot.
$S$	Set containing all subsystems of the branched robot.
$S_i \subset S$	Set of all subsystems that succeed the $i$ th subsystem of the branched robot.
$m_i$	Number of elements in the set $S_i$ .
$i \in S$	The $i$ th subsystem of the branched robot.
$j \in S_i$	Subsystem $j$ that is connected to and succeeds the $i$ th subsystem.
$p_i \in S$	Subsystem $p_i$ that is connected to and precedes the $i$ th subsystem.
$a_i$	Connection point between subsystems $p_i$ and $i$ .
$b_{i,j}$	Connection point between subsystems $i$ and $j \in S_i$ .
$n_i \in \mathbb{N}$	Number of joints/links of the $i$ th subsystem.
$\eta \leq n_i$	Number of joints that precede $b_{i,j}$ in subsystem $i$ .
$n$	Number of rigid bodies of the branched robot.
$\mathcal{Q}, \dot{\mathcal{Q}}, \ddot{\mathcal{Q}}$	Sets containing all the joint configurations, velocities, and accelerations of subsystems that are not black boxes.
$\underline{X}_{p_i,i}$	Vector containing the rigid transformation between the connection point $a_i$ in the preceding subsystem $p_i$ and the CoM of each rigid body within the $i$ th subsystem.
$\underline{X}_{j,i}$	Vector containing the rigid transformation between the connection point $b_{i,j}$ in the succeeding subsystem $j \in S_i$ and the $\eta \leq n_i$ joints of subsystem $i$ .
$\underline{W}_i$	Function that maps the stacked vector of total twists and twist time derivatives at the CoM of each link in the $i$ th subsystem to the corresponding vector of wrenches at the $n_i$ joints.
$\underline{\Xi}_{i,i} \in \mathbb{T}^{2n_i}$	The stacked vector of twists $\underline{\Xi}_{i,i} \in \mathbb{T}^{n_i}$ and twist time derivatives $\dot{\underline{\Xi}}_{i,i} \in \mathbb{T}^{n_i}$ , generated by the $i$ th subsystem, at the $n_i$ CoMs of subsystem $i \in S$ .
$\underline{\Xi}_{p_i,i} \in \mathbb{T}^{2n_i}$	The stacked vector of twists $\underline{\Xi}_{p_i,i} \in \mathbb{T}^{n_i}$ and twist time derivatives $\dot{\underline{\Xi}}_{p_i,i} \in \mathbb{T}^{n_i}$ , expressed in each of the $n_i$ CoMs of subsystem $i$ , resulting from the twist at the connection point $a_i$ .
$\underline{\Xi}_i \in \mathbb{T}^{2n_i}$	The stacked vector of total twists and twists time derivatives at the $n_i$ CoMs of subsystem $i \in S$ (i.e., $\underline{\Xi}_i = \underline{\Xi}_{i,i} + \underline{\Xi}_{p_i,i}$ ).
$\underline{\Gamma}_{j,i} \in \mathbb{W}^\eta$	The vector of wrenches at the $\eta \leq n_i$ joints of subsystem $i$ due to the wrench at the connection point $b_{i,j}$ , with $j \in S_i$ .
$\underline{\hat{\Gamma}}_{j,i} \in \mathbb{W}^{n_i}$	Stacked vector of wrenches, $\underline{\hat{\Gamma}}_{j,i} = \begin{bmatrix} \underline{\Gamma}_{j,i}^T & \mathbf{0}_{n_i-\eta}^T \end{bmatrix}^T \in \mathbb{W}^{n_i}$ , that is used to propagate the wrench at the connection point $b_{i,j}$ to all joints of subsystem $i$ .
$\underline{\Gamma}_i \in \mathbb{W}^{n_i}$	The vector of total wrenches at the $n_i$ joints of subsystem $i \in S$ .
$\underline{\zeta}_{e_\ell}^{\mathcal{L}(\ell)} \in \mathbb{W}$	External wrench at the end-effector indexed by $\mathcal{L}(\ell)$ of leaf subsystem $\ell \in S$ .
$\underline{Z}_e \in \mathbb{W}^\ell$	The vector of external wrenches at the $\ell < s$ end-effectors of the $\ell \in S$ leaf subsystems of the branched robot.
$\underline{\mathbf{0}}_n \in \mathbb{W}^n$	An $n$ -dimensional vector of zeros in the set $\mathbb{W}$ .

Monolithic formulations for the dynamic model of branched robots are not a novelty. Park et al. [7], [8] presented algorithms based on the Lie algebra associated with the Lie group  $SE(3)$  for the dynamic modeling of open-kinematic chains, whereas Featherstone [9], [10] proposed divide-and-conquer algorithms based on spatial algebra, which were later extended by Mukherjee and Anderson [11] to cover flexible bodies. More recent works on the field of branched robots have focused on specific dynamic characterizations such as the analysis of a 5-prismatic–spherical–spherical parallel mechanism [12] and the identification of non-redundant inertial parameters of branched robots [13], contact analysis [14], [15], motion planning [16], [17], and robot design [18].

Nonetheless, there are plenty of motivations for seeking a general formalism for the systematic composition of partial models to obtain the final model of the complete robotic system. One could assemble a robot using existing systems whose dynamic models are already known, such as the limbs of a humanoid robot. In a different scenario, a self-reconfiguring modular robot [19], [20], [21] could possess the dynamic information of its modules that might be reused. From a control perspective, one could be interested in applying distributed control strategies to the subsystems comprising a highly complex dynamic structure composed of thousands of subsystems whose centralized control would be computationally unfeasible. The few works in literature focused on modular composition either require the previous construction of subsystem libraries or demand full knowledge of the dynamic elements of the whole system.

#### A. Related works

The application of linear graph theory in mechanism analysis is not a novelty either, being used to the dynamic modeling of single rigid bodies [22] and multibody systems composed of open [23] and closed kinematic chains [24], [25], [26], [27], [28], [29]. Most approaches lead to different graphs for the rotational and translational variables of the mechanism [22], [30], [23], [26], [28], whereas others focus more on computational [31] and mechanical [32] aspects than on the dynamic modeling of the system. Despite exploring several aspects of graph theory, the aforementioned strategies do not deal with model composition and are, therefore, monolithic.

To overcome the drawbacks of monolithic approaches, Jain [33] proposed a technique of partitioning and aggregating graphs that considers subsystems in the dynamic modeling of multibody systems. Subgraph elements are used to compose the mass matrix and the vector of nonlinear Coriolis and gyroscopic terms of the aggregated system, and then the stacked vector of generalized forces is calculated. Despite the system being composed of individual modules, full knowledge of the masses, inertia tensors, Coriolis accelerations, and gyroscopic terms of the whole system is required.

McPhee et al. [34] presented a strategy that uses individual subsystem models to derive the dynamic model of mechatronic multibody systems. Their approach uses free vectors and rotational matrices, thus decoupling translational and rotational components, which requires separate graphs. Moreover, that

formalism relies on a symbolic implementation, and each subsystem must be symbolically derived before the modeling process for the complete system starts.

Moving away from graph representations, Orsino and Hess-Coelho [35] proposed a strategy for the modular modeling of multibody systems, whose constraints are written as invariants. They use the model of each subsystem to find the constraint equations among the subsystems. Then, the constraint equations are used to obtain the system dynamic equations. Orsino [36] extended that formalism by proposing a hierarchical description of lumped-parameter dynamic systems that lead to a recursive modeling methodology. Albeit both formulations [35], [36] do not impose limitations on how the dynamic equations of each subsystem must be obtained, the final result is not given in terms of the generalized forces or wrenches of the mechanism but rather by a system of differential-algebraic equations of the mechanism's generalized coordinates, constraint equations, and dynamic equations of motion. Thus, those strategies are not readily applicable to robotics problems where one typically needs to find the joint forces/torques as a function of the robot dynamics, which then are used to design suitable control laws. Moreover, both formulations [35], [36] consider that the complete subsystem models are fully available.

More recently, Kumar et al. [37] have proposed a modular solution to the kinematics and dynamics of series-parallel hybrid robots. Their approach consists of a graph representation in which edges correspond to rigid bodies and nodes represent the joints connecting them. The authors use the Lie algebra  $se(3)$  to represent twists and wrenches in the proposed modular recursive Newton-Euler algorithm, achieving a computationally efficient solution. However, the inverse dynamics algorithm does not exploit the system's graph representation with its resultant algebraic operations to find the dynamic model for the whole system. Furthermore, the current formulation cannot handle black-box subsystems since twists and wrenches are explicitly propagated between all subsequent rigid bodies in other subsystems and must be available for all other modules.

Hess-Coelho et al. [38] presented a dynamic modular modeling methodology for parallel mechanisms. They use the hierarchical description proposed by Orsino [36] but follow a different approach to derive the model. Jacobian matrices of the subsystem's angular and linear velocities are used with the Principle of Virtual Power to obtain the Euler-Lagrange model of the robot, and modularity is achieved by using a library of subsystem models. Nonetheless, the process of obtaining such models is highly dependent on geometric analysis of the system (i.e., inverse kinematics) and, if no library containing the subsystems' models is available, the robot dynamics is found monolithically. Moreover, due to the free-vector representation, translational and rotational components are decoupled. As MÅEller [39] pointed out, decoupled representations based on free vectors do not form a group. Therefore, using free vectors doubles the number of equations in the problem; also, one needs to explicitly consider lever arms and their equivalent for velocities and accelerations. In contrast, in formulations with unified representations, those couplings are implicitly

algebraically found thanks to the machinery of group theory.

Yang et al. [40] proposed a modular approach for the dynamic modeling of cable-driven serial robots. They calculate the energy for each component and then apply an energy-based method to integrate the components into the complete model of the robotic system. Their strategy avoids reformulating the coefficient matrix as the number of modules increases but is not applicable to branched robots containing black-box subsystems.

In conclusion, the existing model composition strategies oftentimes generate different graph representations for the translational and rotational components, increasing the overall complexity, and either require the previous construction of subsystem libraries or demand full knowledge of the dynamic elements of the whole system. Some of them also require a symbolic derivation, as opposed to recursive formulations, which makes it harder to model reconfigurable systems. This paper presents a systematic methodology that overcomes those drawbacks. Table I presents a summary of the differences between our proposed formalism and the works in the literature for the dynamic modeling of branched robots.

### B. Statement of contributions

This paper presents the following contributions to the state-of-the-art:

- 1) A strategy for dynamic model composition, shown in Section II, that is applicable even if some subsystems are regarded as black boxes, requiring only the twists, *twist time derivatives*, and wrenches at the connection points between different subsystems. Such information can be obtained either from previous calculations or sensor readings.
- 2) A unified graph representation of the system, shown in Section II-A, that provides the joint wrenches from the calculation of the graph interconnection matrix, in addition to visually depicting the model composition.
- 3) The proposed formulation imposes no restrictions regarding the algebra used to represent twists and wrenches, as long as some basic properties are respected. Nonetheless, we present an instantiation for dual quaternion algebra in Section III.
- 4) A model-based wrench-driven end-effector motion controller, shown in Section IV, allowing to control all end-effectors of the branched robot simultaneously.

We perform numerical evaluations of a fixed-base 24-DOF branched robot and a 30-DoF holonomic branched mobile manipulator. We then compare our results with the ones provided by a realistic simulator and Featherstone's state-of-the-art library for robotic dynamic modeling [3]. To further illustrate how the derived dynamic model can be used in closed-loop control, we also present a simple formulation of a model-based wrench control for branched robots.

This paper is organized as follows: Section II presents the proposed dynamic model composition framework; Section III demonstrates an instantiation of the strategy to dual quaternion algebra; Section IV presents the model-based wrench-driven

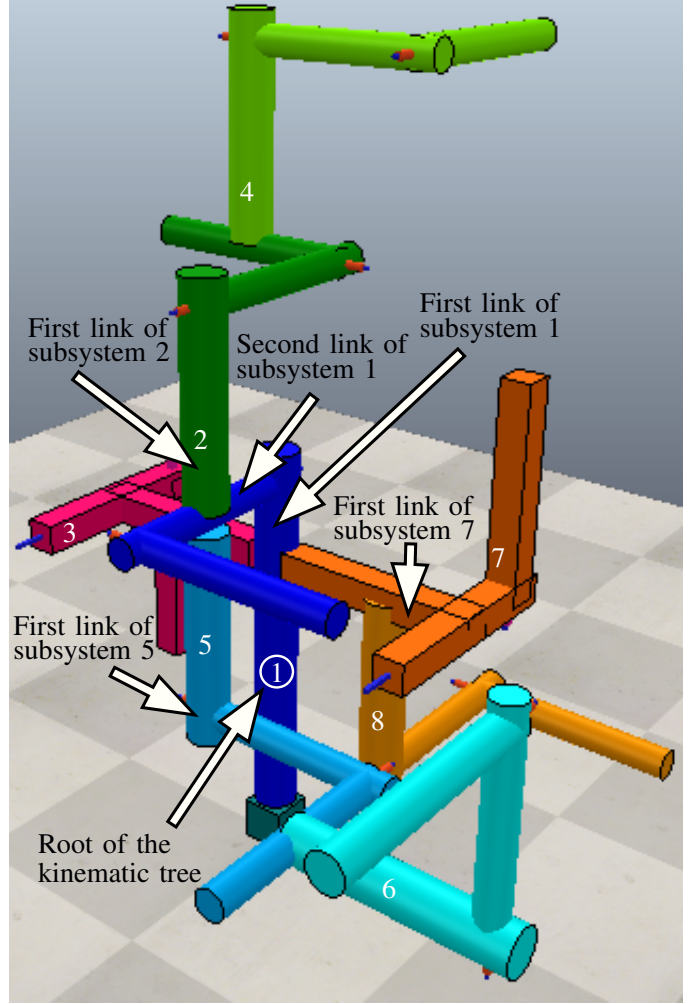


Figure 1: A fixed-base 24-DoF branched manipulator (BM) composed of eight subsystems grouped in different colored links associated with indices from 1 to 8. The root subsystem is indicated by the white circle around index 1.

end-effector motion controller; Section V shows a numerical evaluation of the proposed methodology, and a comparison with a state-of-the-art simulator and state-of-the-art library; Section VI provides the final remarks and points to further research directions; finally, Appendix A briefly reviews the dual quaternion algebra and Appendix B presents the kinematic and dynamic parameters of the robots used in the simulations.

## II. ABSTRACT MODEL COMPOSITION

Consider a branched robot composed of  $s$  subsystems<sup>1</sup> shown in Fig. 1. Given the interconnection points between pair of subsystems and the twists, *twist time derivatives*, and wrenches applied at those points, our goal is to obtain a set of equations that describe the whole-body dynamics as a function of the dynamics of each subsystem  $i \in \{1, \dots, s\} \triangleq S$ .

Given the subsystem  $i \in S$  that immediately precedes and is connected to all  $j \in \{j_{i,1}, \dots, j_{i,m_i}\} \triangleq S_i \subset S$ , we assume that the first link of subsequent subsystems  $j \in S_i$

<sup>1</sup>Subsystems can be defined according to what is convenient for each problem. For instance, they could be a mobile base, a manipulator, an off-the-shelf module, or even another branched robot.

Table I: Summary of the differences between our proposed formalism and the works in literature for the dynamic modeling of branched robots. Check marks (✓) indicate that the topic is covered in the publication, whereas cross marks (×) indicate it is not.

Publication	Graph representation?	Unified graph?	Model composition?	Black-box subsystems?
Park et. al [7], [8]; Featherstone [9], [10]; Mukherjee and Anderson [11]	×	N/A	×	×
Chou et. al [23]; Baciú et. al [26]; McPhee [28]	✓	×	×	×
Sheth and Uicker [24]; Andrews et. al [25]; Hwang and Haug [31]; McPhee [27]; Reungwetwattana and Toyama [29]	✓	✓	×	×
Orsino and Hess-Coelho [35]; Orsino [36]; Althoff et al. [32]; Hess-Coelho et al. [38]; Yang et al. [40]	×	N/A	✓	×
Kumar et al. [37]; Jain [33]; McPhee et al. [34]	✓	✓	✓	×
<b>Our proposed formalism</b>	✓	✓	✓	✓

can be connected to any link of the preceding subsystem  $i$ . For example, in Fig. 1, the first links of subsystem 3 and 7 are connected to the first link of subsystem 1, whereas the first links of subsystems 2 and 5 are connected to the second link of subsystem 1.

Being the complete system an open kinematic tree, each subsystem can only be preceded by one subsystem but can be succeeded by several kinematic chains. Therefore, twists and twist time derivatives generated by the subsystem  $i$  will be propagated to each  $j \in S_i$  and all other subsequent subsystems. On the other hand, the combined wrenches from all  $j \in S_i$  will affect  $i$  and all its preceding subsystems.

Because the forward propagation of twists and twist time derivatives and the backward propagation of wrenches also happen within each subsystem, the idea is similar to the classic Newton-Euler algorithm [41]. Consider that each subsystem  $i \in S$  is composed of  $n_i$  joints/links, is preceded by a subsystem  $p_i \in S$ , and is immediately succeeded by all subsystems  $j \in S_i$ . Also, consider a function

$$\underline{\mathcal{W}}_i : \mathbb{T}^{2n_i} \rightarrow \mathbb{W}^{n_i} \quad (1)$$

that maps the stacked vector  $\underline{\Xi}_i \triangleq \begin{bmatrix} \underline{\Xi}_i^T & \dot{\underline{\Xi}}_i^T \end{bmatrix}^T \in \mathbb{T}^{2n_i}$  of total twists  $\underline{\Xi}_i \in \mathbb{T}^{n_i}$  and twist time derivatives  $\dot{\underline{\Xi}}_i \in \mathbb{T}^{n_i}$  at the center of mass (CoM) of each link in the  $i$ th subsystem to the corresponding vector of total wrenches  $\underline{\Gamma}_i \in \mathbb{W}^{n_i}$  at the  $n_i$  joints.<sup>2</sup> The wrenches at the joints of each subsystem  $i \in S$  originate from three sources: the twists and their time derivatives at the CoMs of each link in the  $i$ th subsystem; the twist and its time derivative at the connection point  $a_i$  with the preceding subsystem  $p_i$ ; and the wrenches at the connection points  $b_{i,j}$  with each  $j \in S_i$ . Therefore,

$$\underline{\Gamma}_i = \underline{\mathcal{W}}_i(\underline{\Xi}_i) + \sum_{j \in S_i} \underline{\Gamma}_{j,i}, \quad \text{with } \underline{\Xi}_i = \underline{\Xi}_{p_i,i} + \underline{\Xi}_{i,i}, \quad (2)$$

where  $\underline{\Xi}_{i,i} \triangleq \begin{bmatrix} \underline{\Xi}_{i,i}^T & \dot{\underline{\Xi}}_{i,i}^T \end{bmatrix}^T \in \mathbb{T}^{2n_i}$  is the stacked vector of twists and twist time derivatives at the  $n_i$  CoMs of subsystem  $i \in S$ ; the elements of  $\underline{\Xi}_{p_i,i} \triangleq \begin{bmatrix} \underline{\Xi}_{p_i,i}^T & \dot{\underline{\Xi}}_{p_i,i}^T \end{bmatrix}^T \in \mathbb{T}^{2n_i}$  are the twists and twist time derivatives at the connection point

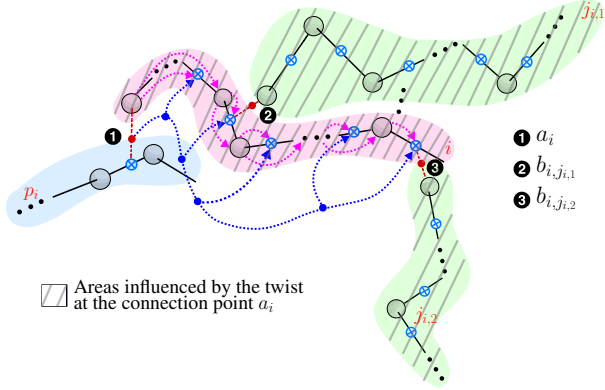
$a_i$  expressed in each of the  $n_i$  CoMs of subsystem  $i$ ; and the elements of  $\underline{\Gamma}_{j,i} \in \mathbb{W}^{n_i}$  are the wrenches of the connection point  $b_{i,j}$  with  $j \in S_i$  expressed in each of the  $\eta \leq n_i$  joints of subsystem  $i$  that precedes  $b_{i,j}$ . More specifically,  $\underline{\Gamma}_{j,i} = \begin{bmatrix} \underline{\Gamma}_{j,i}^T & \underline{\mathbf{0}}_{n_i-\eta}^T \end{bmatrix}^T \in \mathbb{W}^{n_i}$  where  $\underline{\Gamma}_{j,i} \in \mathbb{W}^\eta$  is the vector of wrenches at the  $\eta$  joints preceding the connection point<sup>3</sup>  $b_{i,j}$ , and  $\underline{\mathbf{0}}_{n_i-\eta} \in \mathbb{W}^{n_i-\eta}$  is a vector of zeros in the set  $\mathbb{W}$ . For example, if  $\mathbb{W} = \mathbb{R}^6$ , then  $\underline{\mathbf{0}}_{n_i-\eta} \in \mathbb{W}^{n_i-\eta}$  is equivalent to  $\mathbf{0}_{6(n_i-\eta)} \in \mathbb{R}^{6(n_i-\eta)}$ . If  $\mathbb{W} = \mathcal{H}_p$ , which is the set of pure dual quaternions [42], then  $\mathbf{0}_{n_i-\eta} \in \mathbb{R}^{n_i-\eta}$  because  $\mathcal{H}_p \ni 0 \in \mathbb{R}$  as  $\mathbb{R} \subset \mathcal{H}_p$ .

The wrenches generated at the joints of the  $i$ th subsystem as a result of its own motion, the motion of its predecessor, and the wrenches from its successors is shown in Fig. 2. The connection point  $a_i$  between  $p_i$  and the  $i$ th subsystem, denoted by ❶ in Fig. 2, contains the *resultant* twist generated by all moving joints from the connection point up to the root node. On the other hand, the connection points  $b_{i,j_{i,1}}$  and  $b_{i,j_{i,2}}$  between subsequent kinematic chains connected to the  $i$ th subsystem, respectively denoted by ❷ and ❸ in Fig. 2, contain the *resultant* wrenches generated by those systems and all their successors.

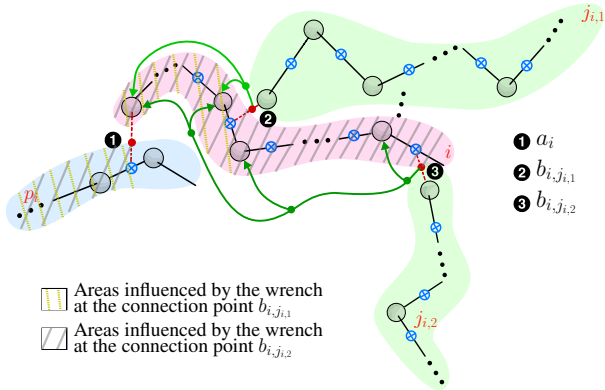
Therefore, to calculate the wrenches at the joints of the  $i$ th subsystem, we need the information of the twists and their time derivatives at its CoMs, the twist and its time derivative at the connection point with its predecessor, and the wrenches at the connection points with its successors. Thus, even when some subsystems are presented as black boxes, the dynamics of the overall system can still be obtained, as long as we have the information of twists, twists derivatives, and wrenches at the connection points (e.g., through sensor readings). This property is particularly relevant in modular robotics applications. For instance, suppose a new, unknown module is appended to a self-reconfiguring robot. The proposed formalism would allow the reconfigurable robot to update its complete dynamic model despite the newly appended black box subsystem as long as wrenches and twists are measured at the connection points. Conversely, methods that require complete knowledge of the

<sup>2</sup>The sets  $\mathbb{W}$  and  $\mathbb{T}$  of wrenches and twists, respectively, are six-dimensional manifolds that can be represented by different algebraic structures, such as six-dimensional spatial vectors [3], four-by-four matrices [4], or pure dual quaternions [42].

<sup>3</sup>Joints after the connection point are not directly affected by wrenches from subsequent subsystems. Nonetheless, because those wrenches will affect the first  $\eta$  joints of the  $i$ th subsystem, the remaining  $n_i - \eta$  links will be indirectly affected because the twists (and their derivatives) at the  $\eta$  joints arising from this interaction will be propagated to the remaining  $n_i - \eta$  links.



(a) Forward propagation of twists from subsystem  $p_i$  to the remaining subsystems of the branched robot. Hatched regions indicate the areas influenced by the twist at the connection point  $a_i$ .



(b) Backward propagation of wrenches from subsystems  $j \in S_i$  to the remaining subsystems of the branched robot. Hatched and crosshatched regions indicate the areas influenced by the wrenches at the connection points  $b_{i,j}$ .

Figure 2: Wrenches generated at the joints of the  $i$ th subsystem (pink region). For each subsystem, the large gray circles represent joints, solid black lines represent links, and blue crossed circles represent CoMs. The preceding subsystem  $p_i$  is given in blue, the subsequent subsystems  $j \in S_i$  are colored in green, and red circles on the red dashed lines, numbered from 1 to 3, indicate the connection points. Dotted arrows represent the forward propagation of twists, whereas solid arrows represent the backward propagation of wrenches.

newly appended module dynamics would be unfit to handle this situation.

**Example 1.** For the sake of simplicity, let us consider only subsystems 1 and 2 in Fig. 1 and disregard the remaining subsystems. In that case, the vectors  $\underline{\Gamma}_1 \in W^{n_1}$  and  $\underline{\Gamma}_2 \in W^{n_2}$  of wrenches at the joints of subsystems 1 and 2, respectively, with  $n_1 = n_2 = 3$ , are given by

$$\begin{aligned} \underline{\Gamma}_1 &= \mathcal{W}_1(\underline{\Xi}_1) + \overset{\circ}{\underline{\Gamma}}_{2,1}, \\ \underline{\Gamma}_2 &= \mathcal{W}_2(\underline{\Xi}_2), \end{aligned} \quad (3)$$

where  $\underline{\Xi}_1 = \underline{\Xi}_{1,1}$  and  $\underline{\Xi}_2 = \underline{\Xi}_{1,2} + \underline{\Xi}_{2,2}$ .

Since subsystem 1 is the first in the chain, the wrenches at its joints are generated by the twists and their time derivatives at the CoMs of its own links, and by the reaction wrenches generated by subsystem 2. On the other hand, for subsystem 2, which is the last in the chain if we disregard the other subsystems, the wrenches at the joints are generated by the

twists and their time derivatives at the CoMs of its own links, in addition to the twist and twist derivative that subsystem 1 contributes through the connection point.

### A. Graph representation

Each subsystem in a branched robot may be represented as a vertex in a graph, in which directed, weighted edges represent the propagation of wrenches, twists, and twist time derivatives. The advantage of such representation is that in addition to visually depicting the model composition, it provides the joint wrenches from the calculation of the graph wrench interconnection matrix. For instance, the weighted graph in Fig. 3 represents the system of Example 1, where dashed edges correspond to the propagation of twists and their time derivatives, and solid edges represent the propagation of wrenches.

The wrench interconnection matrix of the graph presented in Fig. 3 is given by<sup>4</sup>

$$\underline{\mathbf{A}} = [\underline{\mathbf{A}}_{ij}] \triangleq \begin{bmatrix} \mathcal{W}_1(\underline{\Xi}_1) & \overset{\circ}{\underline{\Gamma}}_{2,1} \\ \mathbf{0}_3 & \mathcal{W}_2(\underline{\Xi}_2) \end{bmatrix} \in W^{6 \times 2}, \quad (4)$$

where  $\underline{\Xi}_1 = \underline{\Xi}_{1,1}$  and  $\underline{\Xi}_2 = \underline{\Xi}_{1,2} + \underline{\Xi}_{2,2}$ . The vectors  $\underline{\mathbf{A}}_{ij} \in W^{n_i}$  of the partitioned matrix  $\underline{\mathbf{A}}$  indicate the wrench propagation from vertex  $j$  to vertex  $i$ , represented as a solid edge. Because there is no wrench propagation from subsystem 1 to 2 in Example 1,  $\underline{\mathbf{A}}_{2,1} = \mathbf{0}_3 \in W^3$ , which is a vector of zeros in the set  $W$ . Therefore, since the corresponding “weight” is zero, there is no solid edge from 1 to 2 in the graph on Fig. 3. The wrench interconnection matrix  $\underline{\mathbf{A}}$  is analogous to the weighted adjacency matrix of the graph, but the element  $\underline{\mathbf{A}}_{ij}$  provides the joint wrenches imposed by one subsystem onto another instead of a real scalar weight.

More generally, the graph representation of the complete system composed of  $s$  kinematic chains is constructed as follows:

- 1) Create a vertex for each kinematic chain.
- 2) Add the edges, according to the following rules:
  - a) Each vertex  $i$  has a dashed edge self-loop weighted by its own stacked vector of twists and twist time derivatives  $\underline{\Xi}_{i,i} \in T^{2n_i}$ ;
  - b) Except for the vertex representing the root subsystem of the branched kinematic chain, each vertex  $i$  has an incoming dashed edge from the vertex  $p_i$  representing its predecessor, “weighted” by the stacked vector of twists and twist time derivatives  $\underline{\Xi}_{p_i,i} \in T^{2n_i}$ , and a solid edge self-loop weighted by its own vector of wrenches given by  $\mathcal{W}_i(\underline{\Xi}_{i,i} + \underline{\Xi}_{p_i,i}) \in W^{n_i}$ ;
    - i) If the  $i$ th vertex represents the root subsystem of the branched kinematic chain, then the solid edge self-loop is weighted by  $\underline{\mathcal{W}}_i(\underline{\Xi}_{i,i}) \in W^{n_i}$ .
  - c) Except for the vertex representing the root subsystem of the branched kinematic chain, each vertex  $i$

<sup>4</sup>The interconnection matrix is always  $\underline{\mathbf{A}} \in W^{n \times s}$ , where  $n$  is the total number of rigid bodies in the system and  $s$  is the total number of subsystems of the branched robot.

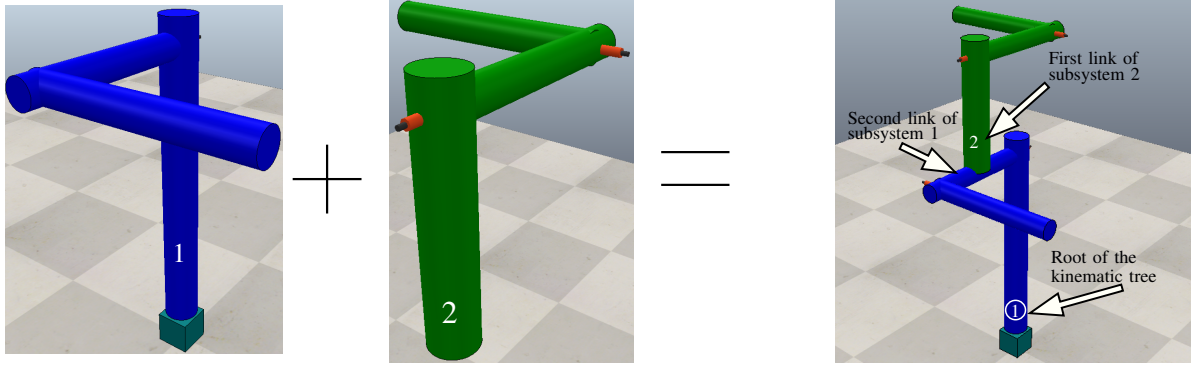


Figure 3: Assembly process of a robot composed of different subsystems: (a) 3-DoF robot given by the first subsystem shown in Fig. 1 and the corresponding graph representation—the wrenches  $\underline{\mathcal{W}}_1(\underline{\Xi}_1)$  of the system are exclusively generated by its own twists and twist time derivatives; (b) 3-DoF robot given by the second subsystem shown in Fig. 1 and its graph representation—the wrenches  $\underline{\mathcal{W}}_2(\underline{\Xi}_{2,2})$  of the system are exclusively generated by its own twists and twist derivatives; (c) 6-DoF assembled robot given by the first two subsystems shown in Fig. 1 and its graph representation. In this combined system, the wrenches of system 2 originates from its twists and twist derivatives  $\underline{\Xi}_{2,2}$  and the twist and twist derivatives  $\underline{\Xi}_{1,2}$  at the connection with system 1. Similarly, the wrenches at the joints of system 1 result from the self-motion wrenches  $\underline{\mathcal{W}}_1(\underline{\Xi}_1)$  of system 1 added by the wrench  $\underline{\Gamma}_{2,1}$  at its connection with system 2.

has an outgoing solid edge that goes to the vertex  $p_i$  representing its predecessor, “weighted” by the vector of wrenches  $\underline{\Gamma}_{i,p_i} \in W^{n_{p_i}}$ .

**Example 2.** Consider the 24-DoF branched robot shown in Fig. 1, where  $n_1 = n_2 = \dots = n_8 = 3$ . Following the procedure described previously, the weighted graph representing this robot is given in Fig. 4. Moreover, the interconnection matrix  $\underline{\mathbf{A}} \in W^{24 \times 8}$  is given by

$$\underline{\mathbf{A}} = \begin{bmatrix} \underline{\mathcal{W}}_1 & \underline{\Gamma}_{2,1} & \underline{\Gamma}_{3,1} & \underline{\mathbf{0}}_3 & \underline{\Gamma}_{5,1} & \underline{\mathbf{0}}_3 & \underline{\Gamma}_{7,1} & \underline{\mathbf{0}}_3 \\ \underline{\mathbf{0}}_3 & \underline{\mathcal{W}}_2 & \underline{\mathbf{0}}_3 & \underline{\Gamma}_{4,2} & \underline{\mathbf{0}}_3 & \underline{\mathbf{0}}_3 & \underline{\mathbf{0}}_3 & \underline{\mathbf{0}}_3 \\ \underline{\mathbf{0}}_3 & \underline{\mathbf{0}}_3 & \underline{\mathcal{W}}_3 & \underline{\mathbf{0}}_3 & \underline{\mathbf{0}}_3 & \underline{\mathbf{0}}_3 & \underline{\mathbf{0}}_3 & \underline{\mathbf{0}}_3 \\ \underline{\mathbf{0}}_3 & \underline{\mathbf{0}}_3 & \underline{\mathbf{0}}_3 & \underline{\mathcal{W}}_4 & \underline{\mathbf{0}}_3 & \underline{\mathbf{0}}_3 & \underline{\mathbf{0}}_3 & \underline{\mathbf{0}}_3 \\ \underline{\mathbf{0}}_3 & \underline{\mathbf{0}}_3 & \underline{\mathbf{0}}_3 & \underline{\mathbf{0}}_3 & \underline{\mathcal{W}}_5 & \underline{\Gamma}_{6,5} & \underline{\mathbf{0}}_3 & \underline{\mathbf{0}}_3 \\ \underline{\mathbf{0}}_3 & \underline{\mathbf{0}}_3 & \underline{\mathbf{0}}_3 & \underline{\mathbf{0}}_3 & \underline{\mathbf{0}}_3 & \underline{\mathcal{W}}_6 & \underline{\mathbf{0}}_3 & \underline{\mathbf{0}}_3 \\ \underline{\mathbf{0}}_3 & \underline{\mathbf{0}}_3 & \underline{\mathbf{0}}_3 & \underline{\mathbf{0}}_3 & \underline{\mathbf{0}}_3 & \underline{\mathbf{0}}_3 & \underline{\mathcal{W}}_7 & \underline{\Gamma}_{8,7} \\ \underline{\mathbf{0}}_3 & \underline{\mathcal{W}}_8 \end{bmatrix},$$

in which

$$\underline{\mathcal{W}}_i = \begin{cases} \underline{\mathcal{W}}_i(\underline{\Xi}_{i,i}) & \text{if } i = 1, \\ \underline{\mathcal{W}}_i(\underline{\Xi}_{p_i,i} + \underline{\Xi}_{i,i}) & \text{if } i \in \{2, \dots, 8\}, \end{cases}$$

$p_2 = p_3 = p_5 = p_7 = 1$ ,  $p_4 = 2$ ,  $p_6 = 5$ , and  $p_8 = 7$ , and  $\underline{\mathbf{0}}_3 \in W^3$  is a vector of zeros in  $W^3$ .

The proposition below shows how the adjacency matrix is used to derive the model of the complete assembled system.

**Proposition 3.** Let a branched kinematic system be composed of  $n$  rigid bodies divided into a set of  $s$  coupled subsystems, each one containing  $n_1, n_2, \dots, n_s$  rigid bodies, respectively. Considering the proposed weighted graph representation with its corresponding adjacency matrix (4), the vector of joint wrenches  $\underline{\Gamma}_{\text{total}}$  of the complete system is given by

$$\underline{\Gamma}_{\text{total}} = [\underline{\Gamma}_1^T \quad \underline{\Gamma}_2^T \quad \dots \quad \underline{\Gamma}_s^T]^T = \underline{\mathbf{A}}\underline{\mathbf{1}}_s \in W^n, \quad (5)$$

where  $\underline{\Gamma}_i \in W^{n_i}$  is the vector of the total joint wrenches of the  $i$ th subsystem,  $\underline{\mathbf{A}} \in W^{n \times s}$  is the interconnection matrix, with  $n = \sum_{i=1}^s n_i$ , and  $\underline{\mathbf{1}}_s \in W^s$  is an  $s$ -dimensional vector of identity elements (under the multiplication operation) in the set  $W$ .

*Proof:* Each block element  $\underline{\mathbf{A}}_{ij} \in W^{n_j}$  of the matrix  $\underline{\mathbf{A}}$  represents the weight of the edge from vertex  $j$  to vertex  $i$  in the interconnection graph and, therefore, the propagation of wrenches from subsystem  $j$  to  $i$ . Hence, each row of  $\underline{\mathbf{A}}$  contains all the wrenches acting upon the joints of the  $i$ th subsystem. Therefore, the vector  $\underline{\Gamma}_i$  of the total joint wrenches of the  $i$ th subsystem is given by  $\underline{\Gamma}_i = \sum_{j=1}^s \underline{\mathbf{A}}_{ij} = \sum_{j=1}^s (\underline{\mathbf{A}}_{ij} \cdot \mathbf{1})$ , where  $\mathbf{1} \in W$  is the identity element in  $W$  under the multiplication operation such that  $\underline{\mathbf{A}}_{ij} \cdot \mathbf{1} = \underline{\mathbf{A}}_{ij}$ . Thus,  $\underline{\Gamma}_{\text{total}} = \underline{\mathbf{A}}\underline{\mathbf{1}}_s$ .<sup>5</sup> ■

Algorithms 1, 2, and 3 summarize the proposed modular dynamic modeling formalism. The inputs for the dynamic modular composition (DMC) algorithm are the sets  $\mathcal{Q}$ ,  $\dot{\mathcal{Q}}$ , and  $\ddot{\mathcal{Q}}$ , respectively, comprised of the joint configurations, velocities, and accelerations of subsystems that are not black boxes. Algorithm 2 presents the forward propagation of the stacked vector of twists and twist time derivatives  $\underline{\Xi} \in T^{2n}$  at the  $n = \sum_{i=1}^s n_i$  CoMs of the robot, in which a breadth-first search (BFS) algorithm is used to traverse the tree [43]. Since the graph representing the topology of the branched robot is constant, we assume it is internally available. Between lines 8 and 11, the twists  $\underline{\Xi}_{i,i}$  are calculated due to the subsystem’s own motion. The implementation of FORWARD\_RECURSION in line 9 depends on the algebra used to represent wrenches and twists. For instance, we provide a formulation using dual quaternion algebra in Algorithm 5. In line 16, the poses  $\underline{\mathbf{X}}_{p_i,j}$  associated with each of the subsystem’s CoMs are calculated as a function of the subsystem’s configuration  $\mathbf{q}_j \in \mathcal{Q}$ .

<sup>5</sup>If  $W = \mathbb{R}^6$  or  $W = \mathcal{H}_p$  (i.e., a pure dual quaternion), then  $\mathbf{1} = 1$  and hence  $\underline{\mathbf{1}}_s = \mathbf{1}_s \in \mathbb{R}^s$ . If  $W \in \text{se}^*(3)$ , then  $\mathbf{1} = \mathbf{I}_{4 \times 4}$  and hence  $\underline{\mathbf{1}}_s \in \mathbb{R}^{4s \times 4}$ .

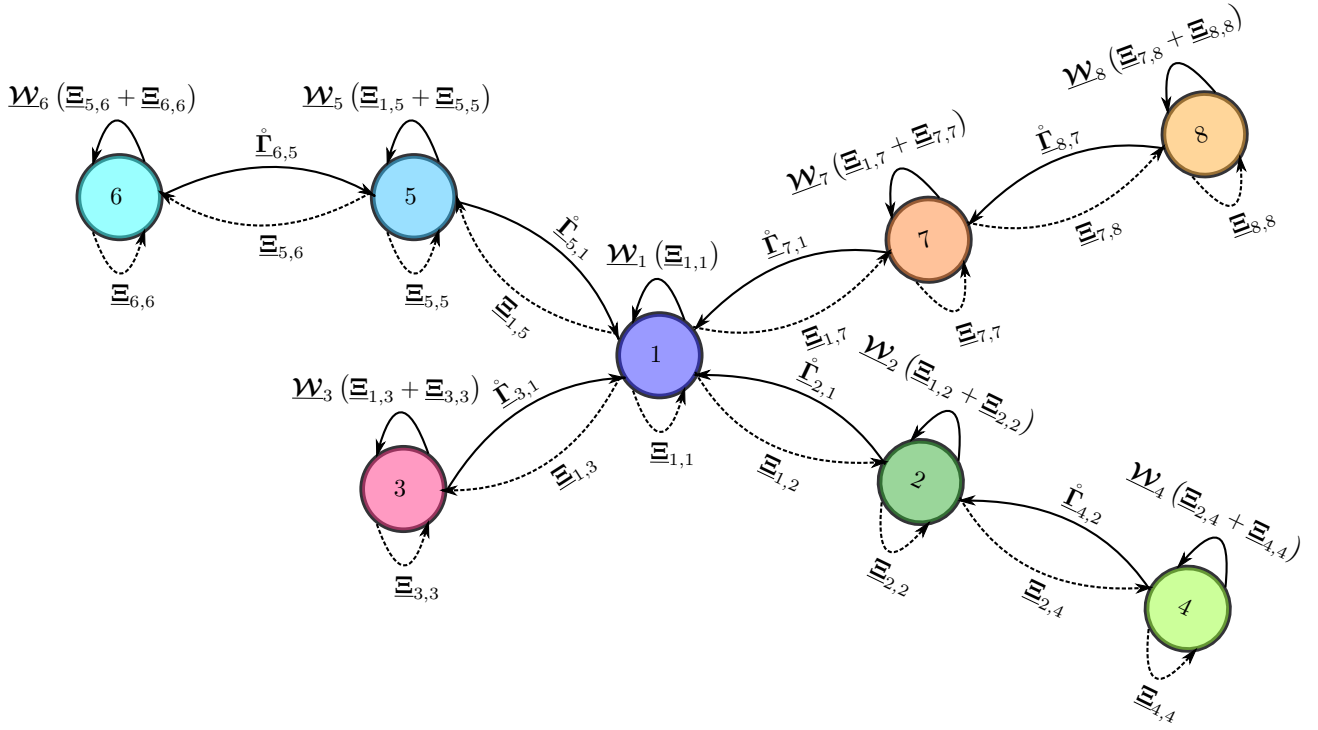


Figure 4: Graph representation of the 24-DoF branched robot. The colored nodes follow the color scheme adopted in Fig. 1. Only the root subsystem, represented by vertex 1, has just one incoming dashed edge, meaning that no twists and twist time derivatives are propagated from other subsystems. On the other hand, only the vertices corresponding to the leaves of the branched system (3, 4, 6, and 8) have only one incoming solid edge, meaning that no wrenches are propagated from other subsystems.

Between lines 12 and 27, the twists  $\underline{\Xi}_{p_j, j}$  due to the preceding subsystem's motion is obtained. If subsystem  $p_j$  is a black box, the twist  $\underline{\xi}_{0, a_j}^{a_j}$  at the connection point  $a_j$  is obtained from sensor readings. Alternatively, the values calculated internally in subsystem  $p_j$  are used to calculate  $\underline{\xi}_{0, a_j}^{a_j}$ .<sup>6</sup> The twist  $\underline{\xi}_{0, a_j}^{a_j}$  is then projected to the appropriate CoM references frames of subsystem  $p_j$ . This operation is also algebra dependent. For dual quaternions, this transformation is given by (6) and (7).

Algorithm 3 calculates the vector  $\underline{\Gamma} \in W^n$  containing the wrenches at the  $n$  joints of the branched robot. For that, the non-zero elements of the interconnection matrix  $\underline{\mathbf{A}}$ , given as in (4), are calculated from right to left. Those are summed to yield each  $\underline{\Gamma}_i \subseteq \underline{\Gamma}$  (i.e.,  $\underline{\Gamma}_i$  is the sum of the coefficients of the  $i$ th row of  $\underline{\mathbf{A}}$ ). Between lines 4 and 6, algorithm  $\underline{\mathcal{N}}$  obtains the wrenches of subsystem  $i$  due to its own motion, whereas between lines 7 and 16 the wrenches that subsystem  $i$  imposes on its preceding subsystem,  $p_i \in S$ , are calculated. The calculation of the relative poses  $\underline{\mathbf{X}}_{j, i}$  and wrenches  $\underline{\Gamma}_{\text{tmp}}$ , and the implementation of  $\underline{\mathcal{W}}_i$  also depend on the algebraic structure representing rigid motions, twists, and wrenches. For instance, when dual quaternion algebra is used, wrench projections are given by (8), whereas  $\underline{\mathcal{W}}_i$  is obtained using Algorithm 7.

<sup>6</sup>If the configuration of subsystem  $p_j$  has not changed, previously calculated and stored values can be used instead of recalculating them.

**Algorithm 1** Dynamic modular composition (DMC) algorithm for a branched robot composed of  $s$  subsystems.

- 1: **function** DMC( $\mathcal{Q}, \dot{\mathcal{Q}}, \ddot{\mathcal{Q}}$ )
- 2:  $(\underline{\mathbf{X}}, \underline{\Xi}, \underline{\Xi}) \leftarrow \text{DMC\_FORWARD\_RECURSION}(\mathcal{Q}, \dot{\mathcal{Q}}, \ddot{\mathcal{Q}})$
- 3:  $\underline{\Gamma} \leftarrow \underline{\mathcal{N}}(\underline{\mathbf{X}}, \underline{\Xi}, \underline{\Xi})$
- 4: **return**  $\underline{\Gamma}$
- 5: **end function**

### III. MODEL COMPOSITION USING DUAL QUATERNION ALGEBRA

The framework presented in Section II is general, has a high level of abstraction, and thus can be instantiated into different mathematical representations. Here we present one instance based on dual quaternion algebra,<sup>7</sup> which is particularly suitable because elements such as unit dual quaternions and pure dual quaternions, when equipped with standard multiplication and addition operations, form Lie groups with associated Lie algebras [5]. Furthermore, dual quaternion algebra provides an elegant and efficient representation of homogeneous transformations [44] and screw theory [45]. Nonetheless, other representations, such as the spatial algebra [3] or the Lie algebra  $se(3)$  [4], might also be used, as long as they capture the high-level operations described in Section II.

Consider the expressions in Section II. If dual quaternions are used, then  $M = T = \mathcal{H}_p$ , where  $\mathcal{H}_p$  is the set of pure dual

<sup>7</sup>Basic definitions are shown in Appendix A. For a more comprehensive introduction of dual quaternion algebra, see [42].

**Algorithm 2** Obtain the twists and their derivatives at the  $n$  CoMs of the  $s$  subsystems.

---

```

1: function DMC_FORWARD_RECURSION( $\mathcal{Q}, \dot{\mathcal{Q}}, \ddot{\mathcal{Q}}$ )
2:    $\Xi_1 \leftarrow (\mathbf{0}_{n_1}, \mathbf{0}_{n_1}), \dots, \Xi_s \leftarrow (\mathbf{0}_{n_s}, \mathbf{0}_{n_s})$ 
3:    $\underline{\mathbf{X}}_{p_1,1} \leftarrow \mathbf{0}_{n_1}, \dots, \underline{\mathbf{X}}_{p_s,s} \leftarrow \mathbf{0}_{n_s}$ 
4:   queue  $\leftarrow 1$  // Initialize the queue
5:   Mark subsystem (1) as visited
6:   while queue is not empty do
7:      $i \leftarrow$  pop first element from queue
8:     if subsystem ( $i$ ) is not black box then
9:        $\Xi_{i,i} \leftarrow$  FORWARD_RECURSION( $q_i, \dot{q}_i, \ddot{q}_i$ )
10:       $\Xi_i \leftarrow \Xi_i + \Xi_{i,i}$ 
11:    end if
12:    for  $j \leftarrow j_{i,1}$  to  $j_{i,m_i}$  do
13:      if  $j$  is unvisited then
14:        Push  $j$  to the end of the queue
15:        if subsystem ( $j$ ) is not black box then
16:          Calculate  $\underline{\mathbf{X}}_{p_j,j}$  using  $a_j$  and  $q_j \in \mathcal{Q}$ 
17:          if subsystem ( $i$ ) is black box then
18:             $\xi_{0,a_j}^{a_j} \leftarrow$  GET_FROM_SENSORS( $i$ )
19:          else
20:            Calculate  $\xi_{0,a_j}^{a_j}$  using  $\Xi_i$ 
21:          end if
22:          Calculate  $\Xi_{p_j,j}$  using  $\xi_{0,a_j}^{a_j}$  and  $\underline{\mathbf{X}}_{p_j,j}$ 
23:           $\Xi_j \leftarrow \Xi_{p_j,j}$ 
24:        end if
25:        Mark subsystem ( $j$ ) as visited
26:      end if
27:    end for
28:  end while
29:   $(\bar{\Xi}, \bar{\Xi}) \leftarrow (\Xi_1, \dots, \Xi_s)$ 
30:   $\underline{\mathbf{X}} \leftarrow (\underline{\mathbf{X}}_{p_1,1}, \dots, \underline{\mathbf{X}}_{p_s,s})$ 
31:  return  $(\underline{\mathbf{X}}, \bar{\Xi}, \dot{\bar{\Xi}})$ 
32: end function

```

---

quaternions; that is, dual quaternions with real part equal to zero (see Appendix A). Also,  $\mathbf{1}_n = \mathbf{1}_n \in \mathbb{R}^n$  and  $\mathbf{0}_n = \mathbf{0}_n \in \mathbb{R}^n$  because  $0, 1 \in \mathbb{R} \subset \mathcal{H}$ , and  $0\mathbf{x} = \mathbf{x}0 = 0$  and  $1\mathbf{x} = \mathbf{x}1 = \mathbf{x}$  for any  $\mathbf{x} \in \mathcal{H}$ . Therefore, the high-level expressions used to propagate twists and wrenches remain unchanged, but the low-level expressions used to express those twists and wrenches in different frames explicitly employ the operations of dual quaternion algebra.

More specifically, the twist  $\xi_{0,a_i}^{a_i} \in \mathcal{H}_p$  at the connection point  $a_i$  between the preceding subsystem  $p_i$  and current subsystem  $i$ , propagated to each of the CoMs of subsystem  $i$ , is given by the vector of twists  $\bar{\Xi}_{p_i,i} \in \mathcal{H}_p^{n_i}$  such that

$$\bar{\Xi}_{p_i,i} = \text{Ad}_{n_i}(\underline{\mathbf{X}}_{p_i,i}) \xi_{0,a_i}^{a_i}, \quad (6)$$

where the (vector) adjoint operator  $\text{Ad}_{n_i}$  is given by (16) and  $\underline{\mathbf{X}}_{p_i,i} = [\mathbf{x}_{a_i}^{c_1} \dots \mathbf{x}_{a_i}^{c_{n_i}}]^T \in \mathcal{S}^{n_i}$  is the vector of the relative poses (i.e., unit dual quaternions) between the connection point  $a_i$  and the  $c_1, \dots, c_{n_i}$  CoMs of the  $i$ th subsystem. The vector of dual quaternions  $\bar{\Xi}_{p_i,i} \in \mathcal{H}_p^{n_i}$  is

**Algorithm 3** Obtain the total joint wrenches of the  $s$  subsystems.

---

```

1: function  $\mathcal{N}(\underline{\mathbf{X}}, \bar{\Xi}, \dot{\bar{\Xi}})$ 
2:    $\Gamma_1 \leftarrow \mathbf{0}_{n_1}, \dots, \Gamma_s \leftarrow \mathbf{0}_{n_s}$ 
3:   for  $i \leftarrow s$  to 1 do
4:     if subsystem ( $i$ ) is not black box then
5:        $\Gamma_i \leftarrow \Gamma_i + \mathcal{W}_i(\Xi_i)$ , with  $\Xi_i \subseteq \bar{\Xi} \cup \dot{\bar{\Xi}}$ 
6:     end if
7:     if subsystem ( $p_i$ ) is not black box then
8:       Calculate  $\underline{\mathbf{X}}_{i,p_i}$  using  $b_{p_i,i}$  and  $\underline{\mathbf{X}}_{p_i,i} \subseteq \underline{\mathbf{X}}$ 
9:       if subsystem ( $i$ ) is black box then
10:         $\zeta_{0,b_{p_i,i}}^{b_{p_i,i}} \leftarrow$  GET_FROM_SENSORS( $i$ )
11:       else
12:        Calculate  $\zeta_{0,b_{p_i,i}}^{b_{p_i,i}}$  using  $\Gamma_i$ 
13:       end if
14:       Calculate  $\Gamma_{\text{tmp}}$  using  $\underline{\mathbf{X}}_{i,p_i}, \zeta_{0,b_{p_i,i}}^{b_{p_i,i}}$ 
15:        $\Gamma_{p_i} \leftarrow \Gamma_{p_i} + \Gamma_{\text{tmp}}$ 
16:     end if
17:   end for
18:    $\Gamma_{\text{total}} \leftarrow (\Gamma_1, \dots, \Gamma_s)$ 
19:   return  $\Gamma_{\text{total}}$ 
20: end function

```

---

given by the time derivative of (6), where each element is given by [46]

$$\frac{d}{dt} \left( \text{Ad}(\mathbf{x}_{a_i}^{c_k}) \xi_{0,a_i}^{a_i} \right) = \text{Ad}(\mathbf{x}_{a_i}^{c_k}) \dot{\xi}_{0,a_i}^{a_i} + \xi_{c_k,a_i}^{c_k} \times \left( \text{Ad}(\mathbf{x}_{a_i}^{c_k}) \xi_{0,a_i}^{a_i} \right), \quad (7)$$

for  $k \in \{1, \dots, n_i\}$ .

Analogously, the wrench  $\zeta_{0,b_{i,j}}^{b_{i,j}} \in \mathcal{H}_p$  at the connection point  $b_{i,j}$  between the current subsystem  $i$  and the succeeding subsystem  $j$ , propagated to each of the CoMs of subsystem  $i$ , is given by the vector of wrenches  $\dot{\Gamma}_{j,i} \in \mathcal{H}_p^{n_i}$  such that<sup>8</sup>

$$\dot{\Gamma}_{j,i} = \text{Ad}_{n_i}(\underline{\mathbf{X}}_{j,i}) \zeta_{0,b_{i,j}}^{b_{i,j}}, \quad (8)$$

in which  $\underline{\mathbf{X}}_{j,i} = \left[ \bar{\mathbf{X}}_{j,i}^T \quad \mathbf{0}_{n_i - \eta}^T \right]^T \in \mathcal{H}^{n_i}$ , with  $\bar{\mathbf{X}}_{j,i} = \left[ \mathbf{x}_{b_{i,j}}^0 \dots \mathbf{x}_{b_{i,j}}^\eta \right]^T \in \mathcal{S}^\eta$  being the vector of relative poses (i.e., unit dual quaternions) between the connection point  $b_{i,j}$  and each of the  $\eta \leq n_i$  joints of subsystem  $i$  that precede  $b_{i,j}$ . Furthermore, the wrench  $\zeta_{0,b_{i,j}}^{b_{i,j}}$  has the form

$$\zeta_{0,b_{i,j}}^{b_{i,j}} = \mathbf{f}_{0,b_{i,j}}^{b_{i,j}} + \varepsilon \tau_{0,b_{i,j}}^{b_{i,j}},$$

where  $\mathbf{f}_{0,b_{i,j}}^{b_{i,j}} = f_x \hat{i} + f_y \hat{j} + f_z \hat{k}$  is the force at the connection point  $b_{i,j}$  given by Newton's second law and  $\tau_{0,b_{i,j}}^{b_{i,j}} = \tau_x \hat{i} +$

<sup>8</sup>It is important to notice that  $\xi_{0,a_i}^{a_i}$  in (6) is the twist at connection point  $a_i$  with respect to frame  $\mathcal{F}_0$ , expressed in frame  $\mathcal{F}_{a_i}$ . Analogously,  $\zeta_{0,b_{i,j}}^{b_{i,j}}$  is the wrench at connection point  $b_{i,j}$  with respect to frame  $\mathcal{F}_0$ , expressed in frame  $\mathcal{F}_{b_{i,j}}$ . We use three indices here because the twist/wrench between two frames can be seen from a third frame. For instance,  $\xi_{a,b}^{a,b}$  is the twist of frame  $\mathcal{F}_b$  with respect to frame  $\mathcal{F}_a$ , expressed in frame  $\mathcal{F}_c$ .

$\tau_y \hat{j} + \tau_z \hat{k}$  is the torque about  $b_{i,j}$  due to the change of its angular momentum, given by the Euler's rotation equation.

Moreover, the function  $\mathcal{W}_i$  is given by (1), in which the sets  $\mathbb{T}$  and  $\mathbb{W}$  are replaced by the set  $\mathcal{H}_p$ , and the low-level dynamic equations of serial kinematic chains using dual quaternions are demonstrated in [46]. Algorithms 4, 5, 6, and 7 summarize the dual quaternion Newton-Euler formalism.<sup>9</sup> It is important to highlight that since these algorithms present the *low-level dynamics* of a subsystem, the indexes used in them correspond to bodies within each subsystem.

**Algorithm 4** Dual Quaternion Newton-Euler Algorithm for a serial mechanism [46]. Vector  $\Gamma \in \mathcal{H}_p^k$  contains the wrenches at each joint of the  $k$ -DOF serial mechanism, whereas  $\Xi \in \mathcal{H}_p^{2k}$  is the stacked vector of twists and twists derivatives at the CoM of each link, and  $q, \dot{q}, \ddot{q}$  are the joint configurations, joint velocities, and joint accelerations, whose dimensions depend on the number of parameters used to represent each joint (e.g., each prismatic or revolute joint adds one dimension, each cylindrical joint adds two, each planar, spherical, and helical joints add three, and each 6-DoF joint adds six dimensions).

```

1: function NEWTON_EULER( $q, \dot{q}, \ddot{q}$ )
2:    $\Xi \leftarrow$  FORWARD_RECURSION( $q, \dot{q}, \ddot{q}$ )
3:    $\Gamma \leftarrow$  BACKWARD_RECURSION( $\Xi$ )
4:   return  $\Gamma$ 
5: end function

```

**Algorithm 5** Forward recursion to obtain the twists and their derivatives for the CoM of all robot links [46]. Each joint  $q_i \in q = (q_1, \dots, q_k)$  and its higher time derivatives are represented by a different number of parameters depending on their type.

```

1: function FORWARD_RECURSION( $q, \dot{q}, \ddot{q}$ )
2:    $\xi_{0,c_0}^{c_0} \leftarrow 0$  and  $\dot{\xi}_{0,c_0}^{c_0} \leftarrow 0$ 
3:   for  $i \leftarrow 1$  to  $k$  do
4:      $(\xi_{i-1,c_i}^{i-1}, \dot{\xi}_{i-1,c_i}^{i-1}) \leftarrow$  JOINT_TWIST( $\dot{q}_i, \ddot{q}_i$ )
5:      $\triangleright$  Calculation of the  $i$ th CoM twist
6:      $\xi_{0,c_i}^{c_i} \leftarrow$  Ad( $\mathbf{x}_{c_{i-1}}^{c_i}$ )  $\xi_{0,c_{i-1}}^{c_{i-1}}$  + Ad( $\mathbf{x}_{i-1}^{c_i}$ )  $\xi_{i-1,c_i}^{i-1}$ 
7:      $\triangleright$  Calculation of the  $i$ -th CoM twist derivative
8:      $\dot{\xi}_{c_i,c_{i-1}}^{c_i} \leftarrow -$  Ad( $\mathbf{x}_{i-1}^{c_i}$ )  $\dot{\xi}_{i-1,c_i}^{i-1}$ 
9:      $\dot{\xi}_{0,c_i}^{c_i} \leftarrow$  Ad( $\mathbf{x}_{c_{i-1}}^{c_i}$ )  $\dot{\xi}_{0,c_{i-1}}^{c_{i-1}}$  + Ad( $\mathbf{x}_{i-1}^{c_i}$ )  $\dot{\xi}_{i-1,c_i}^{i-1}$  +
        $\xi_{c_i,c_{i-1}}^{c_i} \times \left[ \text{Ad} \left( \mathbf{x}_{c_{i-1}}^{c_i} \right) \dot{\xi}_{0,c_{i-1}}^{c_{i-1}} \right]$ 
10:   end for
11:    $\Xi \leftarrow (\xi_{0,c_1}^{c_1}, \dots, \xi_{0,c_k}^{c_k}), \dot{\Xi} \leftarrow (\dot{\xi}_{0,c_1}^{c_1}, \dots, \dot{\xi}_{0,c_k}^{c_k})$ 
12:    $\Xi \leftarrow \begin{bmatrix} \Xi^T \\ \dot{\Xi}^T \end{bmatrix}$ 
13:   return  $\Xi$ 
14: end function

```

The following example illustrates the application of the proposed modular composition strategy to derive the dynamic model of the subsystems 1 and 2 shown in Fig. 1.

<sup>9</sup>For details regarding the algebraic deduction of the equations presented in these algorithms, please refer to [46].

**Algorithm 6** Function to obtain the twists of some of the most commonly used joints in robotics [46].

```

1: function JOINT_TWIST( $\dot{q}_i, \ddot{q}_i$ )
2:   if revolute joint then
3:      $\xi_{i-1,c_i}^{i-1} \leftarrow \omega_i l_i^{i-1}$  and  $\dot{\xi}_{i-1,c_i}^{i-1} \leftarrow \dot{\omega}_i l_i^{i-1}$ 
4:   else if prismatic joint then
5:      $\xi_{i-1,c_i}^{i-1} \leftarrow \varepsilon v_i l_i^{i-1}$  and  $\dot{\xi}_{i-1,c_i}^{i-1} \leftarrow \varepsilon \dot{v}_i l_i^{i-1}$ 
6:   else if spherical joint then
7:      $\xi_{i-1,c_i}^{i-1} \leftarrow \omega_{i_x} \hat{i} + \omega_{i_y} \hat{j} + \omega_{i_z} \hat{k}$ 
8:      $\dot{\xi}_{i-1,c_i}^{i-1} \leftarrow \dot{\omega}_{i_x} \hat{i} + \dot{\omega}_{i_y} \hat{j} + \dot{\omega}_{i_z} \hat{k}$ 
9:   else if planar joint then
10:     $\xi_{i-1,c_i}^{i-1} \leftarrow \omega_i \hat{k} + \varepsilon (v_{i_x} \hat{i} + v_{i_y} \hat{j})$ 
11:     $\dot{\xi}_{i-1,c_i}^{i-1} \leftarrow \dot{\omega}_i \hat{k} + \varepsilon (\dot{v}_{i_x} \hat{i} + \dot{v}_{i_y} \hat{j})$ 
12:   else if cylindrical joint then
13:     $\xi_{i-1,c_i}^{i-1} \leftarrow (\omega_i + \varepsilon v_i) l_i^{i-1}$ 
14:     $\dot{\xi}_{i-1,c_i}^{i-1} \leftarrow (\dot{\omega}_i + \varepsilon \dot{v}_i) l_i^{i-1}$ 
15:   else if helical joint then
16:     $\xi_{i-1,c_i}^{i-1} \leftarrow (\omega_i + \varepsilon h_i \omega_i) l_i^{i-1}$ 
17:     $\dot{\xi}_{i-1,c_i}^{i-1} \leftarrow (\dot{\omega}_i + \varepsilon h_i \dot{\omega}_i) l_i^{i-1}$ 
18:   else if 6-DoF joint then
19:     $\xi_{i-1,c_i}^{i-1} \leftarrow \omega_{i_x} \hat{i} + \omega_{i_y} \hat{j} + \omega_{i_z} \hat{k} + \varepsilon (v_{i_x} \hat{i} + v_{i_y} \hat{j} + v_{i_z} \hat{k})$ 
20:     $\dot{\xi}_{i-1,c_i}^{i-1} \leftarrow \dot{\omega}_{i_x} \hat{i} + \dot{\omega}_{i_y} \hat{j} + \dot{\omega}_{i_z} \hat{k} + \varepsilon (\dot{v}_{i_x} \hat{i} + \dot{v}_{i_y} \hat{j} + \dot{v}_{i_z} \hat{k})$ 
21:   end if
22:   return  $(\xi_{i-1,c_i}^{i-1}, \dot{\xi}_{i-1,c_i}^{i-1})$ 
23: end function

```

**Algorithm 7** Backward recursion to obtain the wrenches at the robot joints [46].

```

1: function BACKWARD_RECURSION( $\Xi$ )
2:    $\zeta_{0,k+1}^k \leftarrow$  external_wrench
3:   for  $i \leftarrow k$  to 1 do
4:      $\xi_{0,c_i}^{c_i} \leftarrow \Xi[i]$  and  $\dot{\xi}_{0,c_i}^{c_i} \leftarrow \dot{\Xi}[i]$ 
5:      $\mathbf{f}_{0,c_i}^{c_i} \leftarrow m_i \left( \mathcal{D} \left( \xi_{0,c_i}^{c_i} \right) + \mathcal{P} \left( \xi_{0,c_i}^{c_i} \right) \times \mathcal{D} \left( \xi_{0,c_i}^{c_i} \right) \right)$ 
6:      $\tau_{0,c_i}^{c_i} \leftarrow \mathcal{L}_3(\mathbb{I}_i^c) \mathcal{P} \left( \xi_{0,c_i}^{c_i} \right) + \mathcal{P} \left( \xi_{0,c_i}^{c_i} \right) \times$ 
        $\left( \mathcal{L}_3(\mathbb{I}_i^c) \mathcal{P} \left( \xi_{0,c_i}^{c_i} \right) \right)$ 
7:      $\zeta_{0,c_i}^{c_i} \leftarrow \mathbf{f}_{0,c_i}^{c_i} + \varepsilon \tau_{0,c_i}^{c_i} - m_i \mathbf{g}^{c_i}$ 
8:      $\triangleright$  Let  $\Gamma[i] = \zeta_{0,c_i}^{i-1}$ 
9:      $\Gamma[i] \leftarrow$  Ad( $\mathbf{x}_{c_i}^{i-1}$ )  $\zeta_{0,c_i}^{c_i} +$  Ad( $\mathbf{x}_i^{i-1}$ )  $\zeta_{0,c_{i+1}}^i$ 
10:   end for
11:   return  $\Gamma$ 
12: end function

```

**Example 4.** Consider Example 1 illustrated in Fig. 3. If dual quaternions are used, then  $\Gamma_1, \Gamma_2 \in W^3 = \mathcal{H}_p^3$ . Also,

$$\hat{\Gamma}_{2,1} = \text{Ad}_3(\mathbf{X}_{2,1}) \zeta_{0,b_{1,2}}^{b_{1,2}},$$

where  $\zeta_{0,b_{1,2}}^{b_{1,2}}$  is the wrench propagated from subsystem 2 to

subsystem 1 at the connection point  $b_{1,2}$ , in which

$$\underline{\mathbf{X}}_{2,1} = \left[ \underline{\mathbf{X}}_{2,1}^T \quad 0 \right]^T = \left[ \underline{\mathbf{x}}_{b_{1,2}}^0 \quad \underline{\mathbf{x}}_{b_{1,2}}^1 \quad 0 \right]^T \in \mathcal{H}^3.$$

The first two elements of  $\underline{\mathbf{X}}_{2,1}$  are different from zero because point  $b_{1,2}$  is connected at the second link of subsystem 1. Therefore,  $\underline{\xi}_{0,b_{1,2}}^{b_{1,2}}$  does not directly affect its last link. Moreover,

$$\underline{\Xi}_{1,2} = \text{Ad}_3(\underline{\mathbf{X}}_{1,2}) \underline{\xi}_{0,a_2}^{a_2},$$

in which  $\underline{\xi}_{0,a_2}^{a_2}$  is the twist propagated from subsystem 1 to subsystem 2 at the connection point  $a_2$ , and

$$\underline{\mathbf{X}}_{1,2} = \left[ \underline{\mathbf{x}}_{a_2}^{\check{c}_1} \quad \underline{\mathbf{x}}_{a_2}^{\check{c}_2} \quad \underline{\mathbf{x}}_{a_2}^{\check{c}_3} \right]^T \in \underline{\mathcal{S}}^3,$$

where the symbol “ $\check{\cdot}$ ” indicates the frames  $\mathcal{F}_{\check{c}_i}$  located at the CoM of each link in subsystem 2 (as opposed to the frames  $\mathcal{F}_{c_i}$  located at the CoM of each link in subsystem 1). Lastly,

$$\underline{\Xi}_{2,2} = \left[ \underline{\xi}_{0,\check{c}_1}^{\check{c}_1} \quad \underline{\xi}_{0,\check{c}_2}^{\check{c}_2} \quad \underline{\xi}_{0,\check{c}_3}^{\check{c}_3} \right]^T \in \mathcal{H}_p^3$$

is the vector of twists at the CoMs of subsystem 2 that are caused exclusively by the motion of the joints of subsystem 2.

#### A. Computational complexity

As presented in [46], Algorithm 4, the dual quaternion Newton-Euler algorithm (dqNE), has a linear cost in the number of DoF of a serial kinematic chain with arbitrary joints. Therefore, each subsystem in the modular composition is calculated with complexity  $O(n_i)$ , where  $n_i$  is the number of DoF of the  $i$ th subsystem.

Algorithm 2, which calculates the twists and their derivatives at the  $n = \sum_{i=1}^s n_i$  CoMs of the  $s$  subsystems, uses a breadth-first search algorithm to traverse all the  $s$  subsystems in the tree. In the worst case when a node is visited, Algorithm 5 is executed once to calculate the forward recursion of dqNE in Line 9 with complexity  $O(n_i)$  and Line 10 is calculated with complexity  $O(2n_i)$  because it correspond to a sum of vectors  $\underline{\Xi}_i, \underline{\Xi}_{i,i} \in \mathcal{T}^{2n_i}$ . Moreover, Line 7 is executed  $s$  times. As such, we have

$$\underbrace{O(s)}_{\text{Line 7}} + \underbrace{O\left(\sum_{i=1}^s n_i\right)}_{\text{Line 9}} + \underbrace{O\left(\sum_{i=1}^s 2n_i\right)}_{\text{Line 10}} = O(s) + O(n) + 2O(n) = O(n),$$

because  $n \geq s$ , as each subsystem has at least one DoF.<sup>10</sup> Additionally, Line 16 is executed  $s-1$  times<sup>11</sup> with complexity  $O(n_j)$ , as we calculate the  $n_j$  elements of  $\underline{\mathbf{X}}_{p_j,j}$ . Furthermore, Line 22 is also executed  $s-1$  times with complexity  $O(n_j)$ ,<sup>12</sup> while the remaining operations between lines 12 to 27 have

<sup>10</sup>We consider the upper bound for the Big  $O$  function [47, p. 47].

<sup>11</sup>In the worse scenario, lines 12 to 27 are calculated for all subsystems, except for root subsystem  $n_1$ .

<sup>12</sup>The twist  $\underline{\xi}_{0,a_j}^{a_j}$  is propagated  $2n_j$  times to generate the vector  $\underline{\Xi}_{p_j,j} \in \mathcal{T}^{2n_j}$ . Moreover,  $O(2n_j) = O(n_j)$ .

constant complexity  $O(1)$  (e.g, dequeuing, reading from a sensor, etc.). Thus, we have

$$\underbrace{O\left(\sum_{j=2}^s n_j\right)}_{\text{Line 16}} + \underbrace{O\left(\sum_{j=2}^s n_j\right)}_{\text{Line 22}} + O((s-1) \cdot 1) = O(n - n_1) + O(n - n_1) + O(s-1) = O(n).$$

Consequently, the complexity of Algorithm 2 is  $O(n) + O(n) = O(n)$ , assuming no black-box subsystems and a centralized computation.

As for Algorithm 3, it traverses matrix  $\underline{\mathbf{A}}$  from right to left. In the worst case, in Line 5, it calls Algorithm 7  $s$  times with complexity  $O(n_i)$  plus it performs  $s$  additions of elements in  $\mathcal{W}^{n_i}$  with complexity  $O(n_i)$ . Thus,

$$O\left(\sum_{i=1}^s n_i\right) + O\left(\sum_{i=1}^s n_i\right) = O(n) + O(n) = O(n).$$

Additionally, between lines 7 and 16, there are  $s-1$  operations with complexity  $O(n_i)$  in lines 8, 14, and 15, and complexity  $O(1)$  in the remaining lines.<sup>13</sup> Consequently,

$$\underbrace{3O\left(\sum_{i=2}^s n_i\right)}_{\text{Lines 8, 14, and 15}} + O(s-1) = 3O(n - n_1) + O(s-1) = O(n)$$

Therefore, the total complexity of Algorithm 3 is  $O(n) + O(n) = O(n)$ .

Consequently, the total complexity of Algorithm 1 is  $O(n) + O(n) = O(n)$ . On the other hand, the complexity of Newton-Euler-based monolithic approaches is also  $O(n)$  [6, p. 51]. This means that the proposed Algorithm 1 allows for modular composition and the inclusion of black box subsystems without incurring a higher complexity even in the worst case. Furthermore, it has the potential to be faster than a monolithic solution with the aid of parallelism. For that, there are plenty of works in the literature regarding parallel BFS algorithms [48], [49], [50], which could be applied to Algorithm 2. Additionally, Algorithm 3 could compute the elements on the columns of matrix  $\underline{\mathbf{A}}$  in parallel for each branch, although information must be synchronized when adding wrenches at points connecting different branches. However, parallelization is out of scope and will be explored in future work.

#### IV. WRENCH-DRIVEN END-EFFECTOR MOTION CONTROL

Advanced general modeling techniques such as the ones in Sections II and III are valuable on their own. Nonetheless, robot dynamic models are more useful if amenable to control design. Therefore, this section illustrates how control laws can be easily designed when using our proposed formalism.

The dual quaternion Newton-Euler formalism for branched robots can be seen as the function  $\underline{\mathcal{N}} : \underline{\mathcal{S}}^n \times \mathcal{H}_p^n \times \mathcal{H}_p^n \rightarrow \mathcal{H}_p^n$  given by

$$\underline{\Gamma} = \underline{\mathcal{N}}\left(\underline{\mathbf{X}}, \underline{\Xi}, \dot{\underline{\Xi}}\right) \in \mathcal{H}_p^n, \quad (9)$$

<sup>13</sup>Only the root subsystem has no precedent subsystem. Thus, in the worse case, lines from 7 to 16 are executed for all subsystems but subsystem 1.

where  $\underline{\Gamma}$  is the vector of wrenches at the  $n$ -DoF branched robot joints,  $\underline{\mathbf{X}} = [\mathbf{x}_{c_1}^0, \dots, \mathbf{x}_{c_n}^0]^T \in \mathcal{S}^n$  is the vector containing the poses associated with each CoM, and  $\underline{\Xi}, \dot{\underline{\Xi}} \in \mathcal{H}_p^n$  are the stacked vector of twists and twist time derivatives at the CoMs, respectively.

The vector  $\underline{\Gamma}$  of the branched robot's joint wrenches can be decomposed into three components,  $\underline{\Gamma} = \underline{\Gamma}_M + \underline{\Gamma}_C + \underline{\Gamma}_g$ , where  $\underline{\Gamma}_M = \mathcal{N}(\underline{\mathbf{X}}, \mathbf{0}_n, \dot{\underline{\Xi}})$  is the vector of joint wrenches due to inertial components,  $\underline{\Gamma}_C = \mathcal{N}(\underline{\mathbf{X}}, \underline{\Xi}, \mathbf{0}_n)$  is the vector of joint wrenches due to Coriolis and Centrifugal effects,  $\underline{\Gamma}_g = \mathcal{N}(\underline{\mathbf{X}}, \mathbf{0}_n, \mathbf{0}_n)$  is the vector of joint wrenches due to gravitational effects, and  $\mathbf{0}_n \in \mathbb{R}^n \subset \mathcal{H}^n$ . The function  $\mathcal{N}$  in (9) is a natural extension from the one used for serial robots [46].

Similarly to Newton-Euler algorithms for serial kinematic chains [46], given the desired wrenches  $\zeta_{e_l}^{\mathcal{L}(l)} \in \mathcal{H}_p$  at the end-effectors of all  $\ell$  leaves, where  $\mathcal{L}(l)$  returns the index of the end-effector frame of the leaf subsystem  $l \in \{1, \dots, \ell\}$ , the stacked vector of external wrenches  $\underline{\mathbf{Z}}_e = [\zeta_{e_1}^{\mathcal{L}(1)}, \dots, \zeta_{e_\ell}^{\mathcal{L}(\ell)}] \in \mathcal{H}_p^\ell$  can be easily propagated during the backward recursion by letting  $\zeta_{0,k+1}^k \leftarrow \zeta_{e_l}^{\mathcal{L}(l)}$  in line 2 of Algorithm 7 for the backward recursion in the  $l$ th leaf subsystem. For that, we first define the function

$$\overline{\mathcal{N}}(\underline{\mathbf{X}}, \underline{\Xi}, \dot{\underline{\Xi}}, \underline{\mathbf{Z}}_e) : \mathcal{S}^n \times \mathcal{H}_p^n \times \mathcal{H}_p^n \times \mathcal{H}_p^\ell \rightarrow \mathcal{H}_p^n, \quad (10)$$

such that  $\underline{\Gamma} = \overline{\mathcal{N}}(\underline{\mathbf{X}}, \underline{\Xi}, \dot{\underline{\Xi}}, \underline{\mathbf{Z}}_e) \in \mathcal{H}_p^n$ . Similarly to (9),  $\overline{\mathcal{N}}(\underline{\mathbf{X}}, \underline{\Xi}, \dot{\underline{\Xi}}, \underline{\mathbf{Z}}_e) = \underline{\Gamma}_M + \underline{\Gamma}_C + \underline{\Gamma}_g + \underline{\Gamma}_Z$ , where  $\underline{\Gamma}_M = \overline{\mathcal{N}}(\underline{\mathbf{X}}, \mathbf{0}_n, \dot{\underline{\Xi}}, \mathbf{0}_s)$ ,  $\underline{\Gamma}_C = \overline{\mathcal{N}}(\underline{\mathbf{X}}, \underline{\Xi}, \mathbf{0}_n, \mathbf{0}_s)$ ,  $\underline{\Gamma}_g = \overline{\mathcal{N}}(\underline{\mathbf{X}}, \mathbf{0}_n, \mathbf{0}_n, \mathbf{0}_s)$ , and  $\underline{\Gamma}_Z = \overline{\mathcal{N}}(\underline{\mathbf{X}}, \mathbf{0}_n, \mathbf{0}_n, \underline{\mathbf{Z}}_e) - \underline{\Gamma}_g$ .

Given the vector of desired poses  $\underline{\mathbf{x}}_d = [\mathbf{x}_{d_1}, \dots, \mathbf{x}_{d_\ell}]^T \in \mathcal{S}^\ell$  at the  $\ell$  leaves' end-effectors, the goal is to design attractive vector fields for  $\underline{\mathbf{Z}}_e \in \mathcal{H}_p^\ell$  to ensure that the vector  $\underline{\mathbf{x}} \in \mathcal{S}^\ell$  of  $\ell$  end-effector poses converge to  $\underline{\mathbf{x}}_d$ . We design  $\underline{\mathbf{Z}}_e$  by using a straightforward extension of the controller presented in [51]. First, given the  $l$ th end-effector pose  $\mathbf{x}_l$ , the desired pose  $\mathbf{x}_{d_l}$ , and the pose error  $\tilde{\mathbf{x}}_l$ , the  $l$ th end-effector twist feedback linearizing control input is given by

$$\underline{\mathbf{U}}_l = -k_p \log \tilde{\mathbf{x}}_l - k_v \tilde{\xi}_l^{\mathcal{L}(l)} + \text{Ad}(\tilde{\mathbf{x}}_l^*) \dot{\xi}_{d_l}^{\mathcal{L}(l)} + \left( \text{Ad}(\tilde{\mathbf{x}}_l^*) \xi_{d_l}^{\mathcal{L}(l)} \right) \times \tilde{\xi}_l^{\mathcal{L}(l)}, \quad (11)$$

where  $\tilde{\xi}_l^{\mathcal{L}(l)} \in \mathcal{H}_p$  is the twist of the  $l$ th leaf end-effector satisfying  $\dot{\tilde{\mathbf{x}}}_l = \frac{1}{2} \tilde{\mathbf{x}}_l \tilde{\xi}_l^{\mathcal{L}(l)}$ , with  $k_p, k_v \in (0, \infty)$  being the controller gains, and  $\xi_{d_l}^{\mathcal{L}(i)}$  and  $\dot{\xi}_{d_l}^{\mathcal{L}(i)}$  are the desired  $l$ th leaf end-effector twist and twist derivatives expressed in the end-effector frame of the  $l$ th leaf [51]. As demonstrated in [51],  $\tilde{\mathbf{x}}_l$  converges asymptotically to 1 when the end-effector error dynamics is given by  $\dot{\tilde{\mathbf{x}}}_l = \frac{1}{2} \tilde{\mathbf{x}}_l \underline{\mathbf{U}}_l$  with  $\underline{\mathbf{U}}_l$  defined as in (11), which implies that  $\mathbf{x}_l \rightarrow \mathbf{x}_{d_l}$  when  $t \rightarrow \infty$ .

Therefore, we define  $\underline{\mathbf{Z}}_e \triangleq [\text{swap}(\underline{\mathbf{U}}_1), \dots, \text{swap}(\underline{\mathbf{U}}_\ell)]^T$  to control the  $\ell$  leaves' end-effectors, where the swap operator defined in Appendix A is used to ensure that the rotational

and linear components of  $\underline{\mathbf{U}}_l$  match the rotational and linear components of  $\zeta_{e_l}^{\mathcal{L}(l)}$  in  $\underline{\mathbf{Z}}_e$ . Using (11) in (10) with  $\underline{\Xi} = \dot{\underline{\Xi}} = \mathbf{0}_n$ , the joint wrench inputs  $\underline{\Gamma}_u$  are given by

$$\underline{\Gamma}_u \triangleq \overline{\mathcal{N}}(\underline{\mathbf{X}}, \mathbf{0}_n, \mathbf{0}_n, \underline{\mathbf{Z}}_e) = \underline{\Gamma}_g + \underline{\Gamma}_Z, \quad (12)$$

where  $\underline{\Gamma}_g$  is the gravity compensation term, and  $\underline{\Gamma}_Z$  is the vector of  $n$  joint wrenches induced by the  $\ell$  end-effector wrenches  $\underline{\mathbf{Z}}_e$  that enforce the end-effector twist feedback linearizing control inputs (11) for all  $l \in \{1, \dots, \ell\}$ . Since the inertial and Coriolis/centrifugal terms in 12 are eliminated, it is equivalent to a feedback-linearizing controller with gravity compensation. Finally, if the robot is composed of revolute and prismatic joints, we obtain the joint forces/torques input  $\tau_u \in \mathbb{R}^n$  by projecting  $\underline{\Gamma}_u \in \mathcal{H}_p^n$  onto the joint motion axes [46].

## V. NUMERICAL EVALUATION AND SIMULATION RESULTS

To evaluate the accuracy and correctness of the model composition methodology proposed in Sections II and III, we performed numerical evaluations using two robots; namely, the fixed-base 24-DoF branched manipulator (BM) shown in Fig. 1 and the 30-DoF holonomic mobile branched manipulator (MBM) shown in Fig. 5. We also include qualitative results to evaluate the wrench-driven end-effector motion control in Section IV.

We implemented the simulations on the robot simulator CoppeliaSim Edu V4.4.0 [52] with the MuJoCo [53] physics engine. The implementation was done in MATLAB 2023b, and the computational library DQ Robotics [54] was used for dual quaternion algebra on a computer running Ubuntu 20.04 LTS 64 bits equipped with an Intel i7-6500u with 8GB RAM.

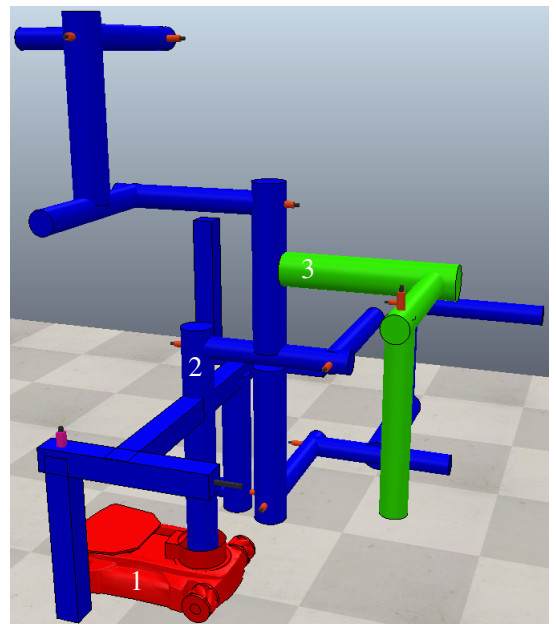


Figure 5: A 30-DoF holonomic mobile branched manipulator (MBM) composed of three subsystems represented by the colored rigid bodies. The second subsystem (blue) is considered as a black box subsystem.

### A. Simulation setup

The BM has eight subsystems, each composed of three DoFs, some containing prismatic or revolute joints. Therefore, the configuration vector is defined as

$$\mathbf{q}_{\text{BM}} = [\mathbf{q}_1^T, \dots, \mathbf{q}_8^T]^T \in \mathbb{R}^{24},$$

with  $\mathbf{q}_1, \dots, \mathbf{q}_8 \in \mathbb{R}^3$ .

Although the MBM is composed of three subsystems, the second one is a black box in our simulation. Thus, the generalized coordinates of the MBM were defined as

$$\mathbf{q}_{\text{MBM}} \triangleq [\check{\mathbf{q}}_1^T \quad \check{\mathbf{q}}_3^T]^T \in \mathbb{R}^6,$$

where  $\check{\mathbf{q}}_1 \triangleq [x_{\text{base}} \quad y_{\text{base}} \quad \phi_{\text{base}}]^T \in \mathbb{R}^3$  is the configuration vector of subsystem 1 (i.e., the holonomic base), with  $x_{\text{base}}$  and  $y_{\text{base}}$  being the Cartesian coordinates and  $\phi_{\text{base}} \in [0, 2\pi)$  being the angle of rotation of the holonomic base. The vector  $\check{\mathbf{q}}_3 \in \mathbb{R}^3$  contains the joint configurations of subsystem 3 in the MBM.

The robots followed arbitrary trajectories in the configuration space, and their configurations ( $\mathbf{q}_{\text{MBM}}$  and  $\mathbf{q}_{\text{BM}}$ ) and configuration velocities ( $\dot{\mathbf{q}}_{\text{MBM}}$  and  $\dot{\mathbf{q}}_{\text{BM}}$ ) were read from CoppeliaSim. Since the simulator does not allow the direct reading of accelerations,  $\dot{\mathbf{q}}_{\text{MBM}}$  and  $\dot{\mathbf{q}}_{\text{BM}}$  were filtered using a discrete filter and used to obtain the configuration accelerations  $\ddot{\mathbf{q}}_{\text{MBM}}$  and  $\ddot{\mathbf{q}}_{\text{BM}}$  by means of numerical differentiation based on Richardson extrapolation [55, p. 322]. Moreover, the generalized torque vectors  $\boldsymbol{\tau}_{\text{MBM}} \in \mathbb{R}^6$  and  $\boldsymbol{\tau}_{\text{BM}} \in \mathbb{R}^{24}$  were also read from CoppeliaSim. For the branches, this information was directly obtained from the joints, whereas for the holonomic base we used a force sensor at the connection point with the first link of the second subsystem.

We used Algorithm 1 to obtain the total wrenches, namely  $\underline{\mathbf{L}}_{\text{BM}} \in \mathcal{H}_p^{24}$  at the BM's joints and  $\underline{\mathbf{L}}_{\text{MBM}} \in \mathcal{H}_p^6$  at the mobile base and joints of MBM's subsystem 3. Afterward, wrenches  $\underline{\mathbf{L}}_{\text{MBM}}$  and  $\underline{\mathbf{L}}_{\text{BM}}$  were projected onto the body motion axes [46] to obtain torques at revolute joints and around the vertical axis of the mobile base, and linear forces at prismatic joints of the branched manipulator and linear motion components of the mobile base.

The comparisons between the generalized force waveforms obtained using the dual quaternion Newton-Euler model composition (dqNEMC) ( $\boldsymbol{\tau}_{\text{MBM}}$  and  $\boldsymbol{\tau}_{\text{BM}}$ ) and the ones read from CoppeliaSim were made considering the **root mean square error (RMSE)** and the **coefficient of multiple correlation (CMC)** [56] between them. The CMC provides a coefficient ranging between zero and one that indicates how similar two given waveforms are. Identical waveforms have CMC equal to one, whereas completely different waveforms have CMC equal to zero. Furthermore, the CMC formulation [56] focuses on assessing the similarity between waveforms acquired synchronously from different models within movement-cycles when the effect of the model on the waveform similarity is the only variable of interest.

Moreover, we also compared our results with the recursive Newton-Euler algorithm (sv2NE) available in Featherstone's

Spatial *v2* package,<sup>14</sup> a widely used and well-established library that implements the robot dynamic modeling based on spatial algebra [3]. Spatial algebra has been used on real complex robotic platforms, such as humanoids, thanks to its good accuracy and computational performance [57]. Therefore, it is a good basis of comparison. However, since the Spatial *v2* package does not support either mobile bases or black box subsystems, we considered the sv2NE only for the fixed-base branched robot. For that simulation, the joint torques  $\boldsymbol{\tau}_{\text{sv2NE}} \in \mathbb{R}^{24}$  were obtained from the sv2NE. Then, we calculated the RMSEs and CMCs between  $\boldsymbol{\tau}_{\text{sv2NE}}$  and the measured joint torques from CoppeliaSim, as well as the RMSEs and CMCs between the joint torques obtained with sv2NE and the dqNEMC.

### B. Model accuracy using the BM

The BM shown in Fig. 1 is composed of eight subsystems. Subsystems 1, 2, 4, 5, 6 and 8 are 3-DoF serial kinematic chains with revolute joints, whereas subsystems 3 and 7 are 3-DoF serial kinematic chains with prismatic joints. Appendix B (see Table IV) presents the kinematic and dynamic information of those subsystems.

The robot joints received sinusoidal position inputs given by  $\mathbf{u}(t) = 0.01 \sin(2\pi t) \mathbf{1}_{24}$  rad, where  $\mathbf{1}_{24} \in \mathbb{R}^{24}$  is a vector of ones. The reference  $\mathbf{u}(t)$  was tracked by CoppeliaSim's internal joint controllers, and the dqNEMC and the sv2NE then receive the *measured* values of  $\mathbf{q}$  and  $\dot{\mathbf{q}}$ . Before being numerically differentiated to obtain  $\ddot{\mathbf{q}}$ , the joint velocities  $\dot{\mathbf{q}}$  were filtered with a second-order discrete low-pass Butterworth filter with normalized cutoff frequency of 100 Hz to filter out measurement noises introduced by CoppeliaSim.

Table II presents the RMSE and the CMC between the joint torque waveforms obtained using dqNEMC and sv2NE and the values obtained from CoppeliaSim, the baseline. Both dqNEMC and sv2NE presented **low mean RMSEs with small standard deviations**. Moreover, dqNEMC and sv2NE also had mean and minimum CMC close to one, with small standard deviation, and high maximum CMC, thus indicating high similarity between the joint torque waveform obtained from dqNEMC, sv2NE, and the values from CoppeliaSim. Moreover, the CMCs between the dqNEMC and the sv2NE are all equal to one, and their RMSE is of the order of  $10^{-14}$ .

Furthermore, the dqNEMC is numerically equivalent to the sv2NE, which demonstrates the accuracy of our proposed strategy when compared to Featherstone's spatial recursive Newton-Euler algorithm. However, it is worth highlighting that the dqNEMC is based on a modular dynamic model of the robot, whereas the sv2NE obtains the joint torques through a monolithic solution (i.e., without considering the existence of subsystems).

For qualitative analysis, Fig. 6 presents the joint torques obtained using dqNEMC and sv2NE, alongside the CoppeliaSim values, for the minimum, maximum, and intermediate CMCs found during simulations. Even for the smallest value of CMC

<sup>14</sup>Available at: <http://royfeatherstone.org/spatial/v2/>

Table II: RMSE and CMC between the joint torque waveforms obtained through different dynamic model strategies and the values obtained from CoppeliaSim for the the 24-DoF branched robot. The closer the CMC is to one, the more similar the waveforms are.

Method	RMSEs for the BM				CMCs for the BM			
	min	max	mean	std	min	max	mean	std
dqNEMC vs. CoppeliaSim	$6.6206 \times 10^{-5}$	0.0364	0.0051	0.0081	0.9888	0.9999	0.9937	0.0037
sv2NE vs. CoppeliaSim	$6.6206 \times 10^{-5}$	0.0364	0.0051	0.0081	0.9888	0.9999	0.9937	0.0037
dqNEMC vs. sv2NE	$1.1041 \times 10^{-16}$	$1.2765 \times 10^{-13}$	$1.695 \times 10^{-14}$	$3.1047 \times 10^{-14}$	1.0000	1.0000	1.0000	0.0000

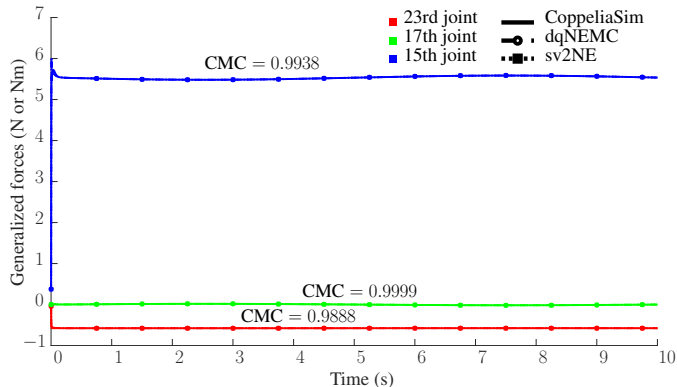


Figure 6: Three joint torques/forces waveforms of the 24-DoF branched robot. *Solid* curves correspond to the CoppeliaSim values, whereas *dashed* curves correspond to the values obtained using the dqNEMC and *dot-dashed* curves correspond to the values obtained using the sv2NE for the joint torque waveforms of the twenty-third (CMC = 0.9888), seventeenth (CMC = 0.9999), and fifteenth (CMC = 0.9938) joints. Because dqNEMC and sv2NE return the same results, the resulting curves for each joint are the same.

(i.e., 0.9888), the joint torques obtained using our model composition formulation match closely the CoppeliaSim values. The small discrepancies arise from discretization effects, small kinematic and dynamic parameters uncertainties, and unmodeled effects in CoppeliaSim, such as friction, measurement noises, and internal controller dynamics.

### C. Model accuracy using the MBM and black-box subsystems

The MBM shown in Fig. 5 is composed of three subsystems, with the second being considered as a black box. The first is a holonomic mobile base, subsystem 2 is the 24-DoF branched manipulator shown in Fig 1, and subsystem 3 consists of a 3-DoF serial mechanism with prismatic joints. Appendix B (see Table IV) presents the kinematic and dynamic information of those subsystems. Subsystems 1 and 3 do not have access to the internal states (joint configurations, joint velocities, and joint accelerations) of Subsystem 2, but the twists, twists derivatives, and wrenches at the connection points are available.

Fig. 7 presents the weighted graph representing the MBM shown in Fig. 5. Although the system has 30 rigid bodies, the 24 rigid bodies of subsystem 2 are inside a black box. Thus, considering only the four known rigid bodies from subsystems 1 and 3 and the fact that we defined three subsystems but the second is a black box, the interconnection matrix  $\underline{A}' \in \mathcal{H}_p^{4 \times 3}$  is given by

$$\underline{A}' = \begin{bmatrix} \underline{W}_1 & \dot{\underline{\Gamma}}_{2,1} & 0 \\ \mathbf{0}_3 & \mathbf{0}_3 & \underline{W}_3 \end{bmatrix}, \quad (13)$$

in which  $\mathbf{0}_3 \in \mathbb{R}^3 \subset \mathcal{H}_p^3$  is a vector of zeros. Furthermore,  $\underline{W}_i = \underline{W}_i(\underline{\Xi}_{i,i})$  when  $i = 1$ , and  $\underline{W}_i = \underline{W}_i(\underline{\Xi}_{p_i,i} + \underline{\Xi}_{i,i})$

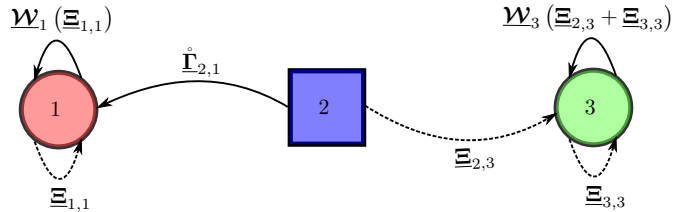


Figure 7: Graph representation of the MBM. The colored nodes follow the color scheme adopted in Fig. 5. The black box subsystem (subsystem 2) is represented by a square, whereas subsystems with available internal information (subsystems 1 and 3) are represented by circles. Despite being a black box, Subsystem 2 has outgoing edges because twists/wrenches are available to neighboring subsystems through sensor readings or direct communication.

when  $i = 3$ , with  $p_2 = 1$  and  $p_3 = 2$ . Notice that, although subsystem 2 is a black box, the wrench  $\underline{\zeta}_{0,b_{1,2}}^{b_{1,2}}$  at the connection point with subsystem 1 is available through direct measurements from a six-axis force sensor.<sup>15</sup> The twist  $\underline{\xi}_{0,p_3}^{p_3}$  and twist derivative  $\dot{\underline{\xi}}_{0,p_3}^{p_3}$  at the connection point between subsystems 2 and 3, which are necessary to calculate  $\underline{\Xi}_{p_3,3}$  in  $\underline{W}_3$ , were obtained directly from CoppeliaSim for simplicity. Nonetheless, this information could be either measured through appropriate sensors or communicated by subsystem 2 after its internal calculations.<sup>16</sup> Therefore,  $\dot{\underline{\Gamma}}_{2,1}$  is calculated using (8), and  $\underline{\Xi}_{p_3,3}$  is calculated using (6) and (7), where  $\underline{X}_{2,1}$  and  $\underline{X}_{p_3,3}$  used in those calculations only require information from subsystem 1 and subsystem 3, respectively.

The robot followed sinusoidal joint/base reference position trajectories given by  $\underline{u}(t) = 0.01 \sin(2\pi t) \mathbf{1}_{30}$  rad, which were tracked by CoppeliaSim's internal joint/base controllers. Notice that the joints of the black-box subsystem 2 are actuated only to simulate possible internal dynamics. However, subsystems 1 and 3 do not have access to this information or the internal states of subsystem 2. Before being used in the model, information obtained from CoppeliaSim ( $\underline{\zeta}_{0,b_{1,2}}^{b_{1,2}}$ ,  $\underline{\xi}_{0,p_3}^{p_3}$  and  $\dot{\underline{q}}$ ) was filtered with a second-order discrete low-pass Butterworth filter with normalized cutoff frequency of 30 Hz. Similarly to the joint accelerations, the twist time derivative  $\dot{\underline{\xi}}_{0,p_3}^{p_3}$  was obtained using numerical differentiation based on Richardson extrapolation.

As explained in Section V-A, the dqNEMC then receives the values of  $\underline{q}$ ,  $\dot{\underline{q}}$ , and  $\ddot{\underline{q}}$ . The comparison is made considering the generalized forces  $\underline{\tau}$  read from the joints and the force sensor

<sup>15</sup>The information propagated by the Newton-Euler algorithm (Algorithm 4) relates to joint actuation torques rather than to reaction torques at the joints. Thus, the torque  $\underline{\zeta}_{0,b_{1,2}}^{b_{1,2}}$  is the opposite of the value read from the sensor (i.e.,  $\underline{\zeta}_{0,b_{1,2}}^{b_{1,2}} = -\underline{\zeta}_{\text{sensor}}^{b_{1,2}}$ ).

<sup>16</sup>Because subsystem 2 is a black box, its internal states cannot be accessed. Nonetheless, the connection points can be regarded as the outputs of black-box subsystems.

at the base.

Table III presents the RMSE and the CMC between the joint torque waveforms obtained through the dqNEMC and the values obtained from CoppeliaSim. As with the previous simulation, the dqNEMC presented low RMSEs and mean and minimum CMC close to one, with small standard deviation, and high maximum CMC, thus indicating high similarity between the joint torque waveform obtained from dqNEMC and the values from CoppeliaSim.

For qualitative analysis, Fig. 8 presents the joint torques obtained using dqNEMC alongside the CoppeliaSim values, for the minimum, maximum, and intermediate CMCs found during simulations. Even for the smallest value of CMC (i.e., 0.9498), the joint torques obtained using our model composition formulation match closely the CoppeliaSim values. The small discrepancies arise from discretization, unmodeled effects in CoppeliaSim, and small uncertainties in the kinematic and dynamic models.

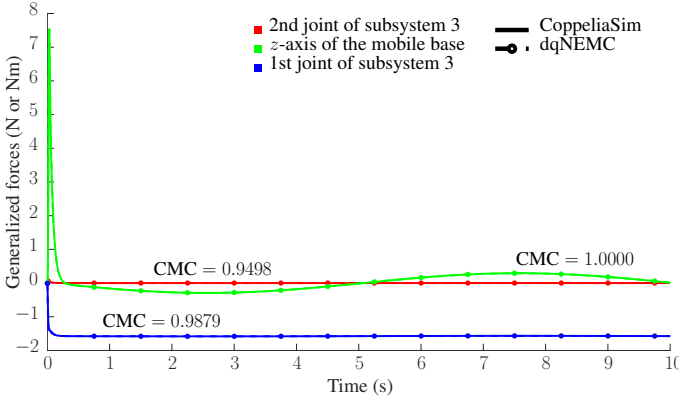


Figure 8: Torque waveforms for three joints of the MBM. Solid curves correspond to the CoppeliaSim values, whereas dashed curves with circle markers correspond to the values obtained using the dqNEMC for the joint torque waveforms of the first (CMC = 0.9879) and second (CMC = 0.9498) joints of subsystem 3 and the generalized force along the  $z$ -axis of subsystem 1 (CMC = 1.0000).

#### D. Closed-loop control of the MBM

Consider the MBM shown in Fig. 5. However, rather than considering the whole BM as a black box subsystem, we consider all its eight subsystems explicitly as we want to control the robot. As a result, the MBM consists of 10 subsystems in this simulation. Subsystem 1 in Fig 5 is the root node and is attached to subsystem 1 from the BM, which is now labeled subsystem 2. Consequently, all subsystem labels shown in Fig. 1 are increased by one. Finally, subsystem 10 is attached to the first link of the new subsystem 3 (previously labeled subsystem 2 in Fig. 1).

Using (12), we control the end-effector pose of the  $\ell$  leaf subsystems of the MBM. Subsystems 4, 5, 9, and 10 received desired end-effector poses within their workspace, whereas desired pose of subsystem 7 was given by its initial end-effector pose.

Fig. 9 shows the norm of the pose error for all leaf subsystems' end-effectors, each given by  $\|\tilde{\mathbf{y}}_l\|_2$  with  $\tilde{\mathbf{y}}_l =$

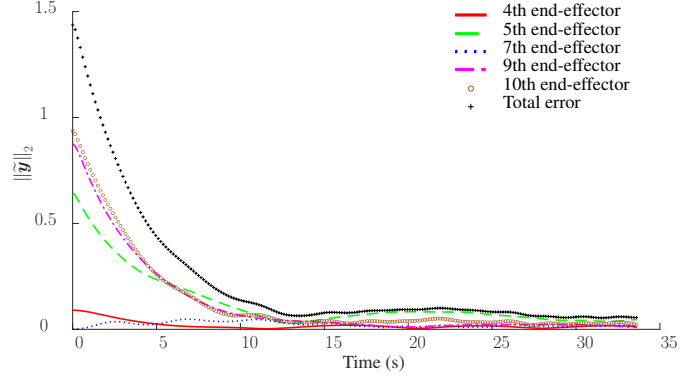


Figure 9: Norm of the closed loop error response for the end-effectors of the  $\ell$  leaf subsystems of the MBM. The solid red curve, the dashed green curve, the blue dotted curve, the magenta dash-dotted curve, and the circled brown curve correspond, respectively, to the end-effectors of subsystems 4, 5, 7, 9, and 10, whereas the crossed black curve corresponds to the norm of the total error (14).

$\text{vec}_6(\log \tilde{\mathbf{x}}_l)$  for all  $l \in \{4, 5, 7, 9, 10\}$ , and the norm of the total error given by  $\|\tilde{\mathbf{y}}\|_2$  where

$$\tilde{\mathbf{y}} = [\tilde{\mathbf{y}}_4^T \quad \tilde{\mathbf{y}}_5^T \quad \tilde{\mathbf{y}}_7^T \quad \tilde{\mathbf{y}}_9^T \quad \tilde{\mathbf{y}}_{10}^T]^T. \quad (14)$$

The oscillatory behavior of the error response is expected because the desired closed-loop error dynamics for the end-effector poses due to control law (11) is described by a second-order system [51]. Nonetheless, the error for the end-effector poses of all subsystems decay and achieve steady-state.

## VI. CONCLUSIONS

This paper has presented a modular composition strategy for the dynamic modeling of branched robots that provides a high level of abstraction and enables combining the dynamics of simpler mechanisms to obtain the whole-body dynamics. The proposed formalism requires only twists, twist time derivatives, and wrenches at the connection points between different subsystems to find the coupled dynamics of the combined mechanisms. Thus, distinct from other approaches in the literature, our strategy works even when subsystems are black boxes, as long as the required information at the connection points is known, which can be done through sensor readings. This property is particularly appealing in modular robotics, where different independent kinematic structures can be arbitrarily combined, making the preprogramming of dynamic modeling equations for the whole system impractical. Furthermore, we also proposed a graph representation for the complete branched mechanism, where each vertex is an open kinematic chain, and the wrenches at the joints result from the graph interconnection matrix. This representation enables obtaining the dynamics of the whole system through straightforward algebraic operations. Moreover, all these features are achieved, in the worst case, with the same linear complexity in the number of DoFs as well-established monolithic recursive Newton-Euler algorithms. Additionally, we have presented a formulation for wrench-driven end-effector motion control to illustrate the applicability of the model obtained through the recursive equations of the dynamic model decomposition.

Table III: RMSE and CMC between the joint torque waveforms obtained through the dqNEMC and the values obtained from CoppeliaSim for the 30-DoF holonomic branched robot. The closer the CMC is to one, the more similar the waveforms are.

Method	RMSEs for the MBM				CMCs for the MBM			
	min	max	mean	std	min	max	mean	std
dqNEMC	0.0004	0.3917	0.0697	0.1578	0.9498	1.0000	0.9856	0.0199

Simulation results have shown that our strategy is numerically equivalent to monolithic solutions, such as Featherstone's Spatial v2 Newton-Euler algorithm, whose dynamic model is built considering the whole open kinematic tree at once and assumes full knowledge of twists, twists derivatives, and wrenches acting on all rigid bodies in the multibody system. Those results have also shown that our formalism can be effectively used to obtain the dynamic model of a branched mobile manipulator containing a large black box subsystem. Indeed, the values of joint torques in non-black systems closely matched the ones given by the simulator, as attested by high CMCs, with small discrepancies arising solely due to unmodeled effects (e.g., measurement noise in CoppeliaSim and discretization effects). Furthermore, the numerical results for the motion control of the end-effectors of a robot composed of a branched kinematic structure on top of a holonomic base show that our model can be used for control design.

Future work will focus on extending the proposed formulation to closed kinematic chains and exploiting parallelization techniques for real-time calculation of the dynamic model of complex branched robots with a very large number, potentially thousands of degrees of freedom. We intend to explore applications in self-reconfiguring robots, in which the method must handle the inclusion or removal of possible unknown modules at execution time. Lastly, we will also expand the control formulation to handle conflicting desired wrenches and geometric constraints across the kinematic tree.

#### APPENDIX A

##### DUAL QUATERNION ALGEBRA

Dual quaternions [5] are elements of the set

$$\mathcal{H} \triangleq \{\mathbf{h}_P + \varepsilon \mathbf{h}_D : \mathbf{h}_P, \mathbf{h}_D \in \mathbb{H}, \varepsilon \neq 0, \varepsilon^2 = 0\},$$

where  $\mathbb{H} \triangleq \{h_1 + \hat{i}h_2 + \hat{j}h_3 + \hat{k}h_4 : h_1, h_2, h_3, h_4 \in \mathbb{R}\}$  is the set of quaternions, in which  $\hat{i}$ ,  $\hat{j}$  and  $\hat{k}$  are imaginary units with the properties  $\hat{i}^2 = \hat{j}^2 = \hat{k}^2 = \hat{i}\hat{j}\hat{k} = -1$  [5]. Addition and multiplication of dual quaternions are analogous to their counterparts of real and complex numbers. One must only respect the properties of the dual unit  $\varepsilon$  and imaginary units  $\hat{i}, \hat{j}, \hat{k}$ . Given  $\underline{\mathbf{h}} \in \mathcal{H}$ , with  $\underline{\mathbf{h}} = \mathbf{h}_P + \varepsilon \mathbf{h}_D$ , we define swap :  $\mathcal{H} \rightarrow \mathcal{H}$  such that  $\text{swap}(\underline{\mathbf{h}}) \triangleq \mathbf{h}_D + \varepsilon \mathbf{h}_P$ .

The subset  $\mathcal{S} = \{\underline{\mathbf{h}} \in \mathcal{H} : \|\underline{\mathbf{h}}\| = 1\}$  of unit dual quaternions, where  $\|\underline{\mathbf{h}}\| = \sqrt{\underline{\mathbf{h}}\underline{\mathbf{h}}^*} = \sqrt{\mathbf{h}^*\mathbf{h}}$ , with  $\underline{\mathbf{h}}^*$  being the conjugate of  $\underline{\mathbf{h}}$  [42], is used to represent poses (position and orientation) in the three-dimensional space and form the group  $\text{Spin}(3) \ltimes \mathbb{R}^3$  under the multiplication operation. Any  $\underline{\mathbf{x}} \in \mathcal{S}$  can always be written as  $\underline{\mathbf{x}} = \mathbf{r} + \varepsilon(1/2)\mathbf{p}\mathbf{r}$ , where  $\mathbf{p} = \hat{i}x + \hat{j}y + \hat{k}z$  represents the position  $(x, y, z)$  and  $\mathbf{r} = \cos(\phi/2) + \mathbf{n} \sin(\phi/2)$  represents a rotation, in which  $\phi \in [0, 2\pi)$  is the rotation angle around the rotation axis  $\mathbf{n} \in \mathbb{H}_P \cap \mathbb{S}^3$ , with  $\mathbb{H}_P \triangleq \{\mathbf{h} \in \mathbb{H} : \text{Re}(\mathbf{h}) = 0\}$ , where  $\text{Re}(h_1 + \hat{i}h_2 + \hat{j}h_3 + \hat{k}h_4) \triangleq$

$h_1$ , and  $\mathbb{S}^3 = \{\mathbf{h} \in \mathbb{H} : \|\mathbf{h}\| = 1\}$  [5]. Given  $\underline{\mathbf{x}} \in \mathcal{S}$ , the logarithmic mapping is defined as  $\log \underline{\mathbf{x}} \triangleq (\phi \mathbf{n} + \varepsilon \mathbf{p})/2$ .

The set  $\mathcal{H}_P = \{\underline{\mathbf{h}} \in \mathcal{H} : \text{Re}(\underline{\mathbf{h}}) = 0\}$  of pure dual quaternions is used to represent twists and wrenches, which are represented in different coordinate systems using the adjoint operator  $\text{Ad} : \mathcal{S} \times \mathcal{H}_P \rightarrow \mathcal{H}_P$ . For instance, consider the twist  $\underline{\xi}^a \in \mathcal{H}_P$  expressed in frame  $\mathcal{F}_a$  and the unit dual quaternion  $\underline{\mathbf{x}}_a^b = \mathbf{r}_a^b + \varepsilon \frac{1}{2} \mathbf{r}_a^b \mathbf{p}_{b,a}^a$  that represents the rigid motion from  $\mathcal{F}_b$  to  $\mathcal{F}_a$ . The same twist is expressed in frame  $\mathcal{F}_b$  as

$$\underline{\xi}^b = \text{Ad}(\underline{\mathbf{x}}_a^b) \underline{\xi}^a = \underline{\mathbf{x}}_a^b \underline{\xi}^a (\underline{\mathbf{x}}_a^b)^*, \quad (15)$$

where  $\underline{\xi}^a = \omega_{b,a}^a + \varepsilon \dot{\mathbf{p}}_{b,a}^a$  and  $\underline{\xi}^b = \omega_{b,a}^b + \varepsilon (\dot{\mathbf{p}}_{b,a}^b + \mathbf{p}_{b,a}^b \times \omega_{b,a}^b)$ , and  $\omega_{b,a}^a, \omega_{b,a}^b \in \mathbb{H}_P$  are the angular velocities that satisfy  $\dot{\mathbf{r}}_a^b = \frac{1}{2} \omega_{b,a}^b \mathbf{r}_a^b = \frac{1}{2} \mathbf{r}_a^b \omega_{b,a}^a$  [42]. Wrenches are represented analogously but with the linear force in the primary part and the moment in the dual part [58]. For instance, given the wrench  $\underline{\zeta}^a = \mathbf{f}^a + \varepsilon \mathbf{m}^a$  in frame  $\mathcal{F}_a$ , with  $\mathbf{f}^a, \mathbf{m}^a \in \mathbb{H}_P$ , it can be expressed in frame  $\mathcal{F}_b$  through the transformation  $\underline{\zeta}^b = \text{Ad}(\underline{\mathbf{x}}_a^b) \underline{\zeta}^a$ . Given  $\underline{\mathbf{h}}_p \in \mathcal{H}_P$ , such that  $\underline{\mathbf{h}}_p = h_1 \hat{i} + h_2 \hat{j} + h_3 \hat{k} + \varepsilon (h_4 \hat{i} + h_5 \hat{j} + h_6 \hat{k})$ , it can be mapped to  $\mathbb{R}^6$  by using  $\text{vec}_6(\underline{\mathbf{h}}_p) \triangleq [h_1 \ h_2 \ h_3 \ h_4 \ h_5 \ h_6]^T$ .

The next definition extends the adjoint operation (15) to the set  $\mathcal{H}_P^n$ .

**Definition 5.** Given a vector of poses  $\underline{\mathbf{X}} = [\underline{\mathbf{x}}_1 \ \underline{\mathbf{x}}_2 \ \dots \ \underline{\mathbf{x}}_n]^T \in \mathcal{S}^n$  and a pure dual quaternion  $\underline{\mathbf{a}} \in \mathcal{H}_P$ , the operator  $\text{Ad}_n : \mathcal{S}^n \times \mathcal{H}_P \rightarrow \mathcal{H}_P^n$  is defined as

$$\begin{aligned} \text{Ad}_n(\underline{\mathbf{X}}) \underline{\mathbf{a}} &\triangleq \text{diag}(\underline{\mathbf{X}}) \underline{\mathbf{a}} \underline{\mathbf{X}}^{*T} \\ &= [\text{Ad}(\underline{\mathbf{x}}_1) \underline{\mathbf{a}} \quad \text{Ad}(\underline{\mathbf{x}}_2) \underline{\mathbf{a}} \quad \dots \quad \text{Ad}(\underline{\mathbf{x}}_n) \underline{\mathbf{a}}]^T \end{aligned} \quad (16)$$

where  $\text{diag}(\underline{\mathbf{X}}) \in \mathcal{H}_P^{n \times n}$  is a diagonal matrix with the elements of  $\underline{\mathbf{X}}$  in the main diagonal, and  $\underline{\mathbf{X}}^*$  is the conjugate transpose of  $\underline{\mathbf{X}}$ .

#### APPENDIX B

##### ROBOT PARAMETERS

Table IV presents the kinematic and dynamic parameters of the 3-DoF manipulators with revolute/prismatic joints and the holonomic mobile base used in the branched robots shown in Figs. 1 and 5.

#### REFERENCES

- [1] B. Siciliano, L. Sciacicco, L. Villani, and G. Oriolo, *Robotics*. London: Springer London, 2009. [Online]. Available: <http://link.springer.com/10.1007/978-1-84628-642-1>
- [2] M. W. Spong, S. Hutchinson, and M. Vidyasagar, *Robot Modeling and Control*. New York, NY: Wiley, 2006.
- [3] R. Featherstone, *Rigid Body Dynamics Algorithms*. New York, NY: Springer, 2008.

Table IV: Kinematic and dynamic information of the robots used in simulation.

Link	D-H parameters				CoM	Mass (Kg)	Inertia tensor ( $\mathbb{I} \triangleq (\hat{i}_x, \hat{i}_y, \hat{i}_z) \in \mathbb{H}_p^3$ )
	$a_i$	$\alpha_i$	$d_i$	$\theta_i$			
<b>3-DoF manipulators with revolute/prismatic joints</b>							
1	0	$\frac{\pi}{2}$	0.187	$\frac{\pi}{2}$	$-0.187\hat{j}$	0.8	$\hat{i}_x = 0.80\hat{i}, \hat{i}_y = 0.80\hat{j}, \hat{i}_z = 0.80\hat{k}$
2	0	$\frac{\pi}{2}$	0.43	$\frac{\pi}{2}$	$-0.195\hat{j}$	0.5	$\hat{i}_x = 0.50\hat{i}, \hat{i}_y = 0.50\hat{j}, \hat{i}_z = 0.50\hat{k}$
3	0	0	0	0	$0.235\hat{k}$	0.10	$\hat{i}_x = 0.10\hat{i}, \hat{i}_y = 0.10\hat{j}, \hat{i}_z = 0.10\hat{k}$
<b>Holonomic mobile base</b>							
N/A	N/A	N/A	N/A	N/A	0	80	$\hat{i}_x = 40\hat{i}, \hat{i}_y = 40\hat{j}, \hat{i}_z = 40\hat{k}$

- [4] R. M. Murray, Z. Li, and S. S. Sastry, *A Mathematical Introduction to Robotic Manipulation*. CRC Press, 1994.
- [5] J. M. Selig, *Geometric Fundamentals of Robotics*, D. Gries and F. B. Schneider, Eds. New York, NY: Springer New York, 2005.
- [6] B. Siciliano and O. Khatib, *Springer Handbook of Robotics*, B. Siciliano and O. Khatib, Eds. Berlin, Heidelberg: Springer Berlin Heidelberg, 2008. [Online]. Available: <http://link.springer.com/10.1007/978-3-540-30301-5>
- [7] F. Park, J. Bobrow, and S. Ploen, "A Lie Group Formulation of Robot Dynamics," *The International Journal of Robotics Research*, vol. 14, no. 6, pp. 609–618, Dec. 1995. [Online]. Available: <http://journals.sagepub.com/doi/10.1177/027836499501400606>
- [8] F. C. Park, B. Kim, C. Jang, and J. Hong, "Geometric Algorithms for Robot Dynamics: A Tutorial Review," *Applied Mechanics Reviews*, vol. 70, no. 1, p. 010803, Jan. 2018. [Online]. Available: <https://asmedigitalcollection.asme.org/appliedmechanicsreviews/article/70/1/010803/443696/Geometric-Algorithms-for-Robot-Dynamics-A-Tutorial>
- [9] R. Featherstone, "A Divide-and-Conquer Articulated-Body Algorithm for Parallel O(log(n)) Calculation of Rigid-Body Dynamics. Part 1: Basic Algorithm," *The International Journal of Robotics Research*, vol. 18, no. 9, pp. 867–875, Sep. 1999. [Online]. Available: <http://journals.sagepub.com/doi/10.1177/02783649922066619>
- [10] —, "A Divide-and-Conquer Articulated-Body Algorithm for Parallel O(log(n)) Calculation of Rigid-Body Dynamics. Part 2: Trees, Loops, and Accuracy," *The International Journal of Robotics Research*, vol. 18, no. 9, pp. 876–892, Sep. 1999. [Online]. Available: <http://journals.sagepub.com/doi/10.1177/02783649922066628>
- [11] R. M. Mukherjee and K. S. Anderson, "A Logarithmic Complexity Divide-and-Conquer Algorithm for Multi-flexible Articulated Body Dynamics," *Journal of Computational and Nonlinear Dynamics*, vol. 2, no. 1, pp. 10–21, Jan. 2007. [Online]. Available: <https://asmedigitalcollection.asme.org/computationalnonlinear/article/2/1/10/464858/A-Logarithmic-Complexity-Divide-and-Conquer>
- [12] Y. Li, H. Zheng, B. Chen, P. Sun, Z. Wang, K. Shuai, and Y. Yue, "Dynamic Modeling and Analysis of 5-PSS/UPU Parallel Mechanism with Elastically Active Branched Chains," *Chinese Journal of Mechanical Engineering*, vol. 33, no. 1, p. 44, Dec. 2020. [Online]. Available: <https://cjme.springeropen.com/articles/10.1186/s10033-020-00460-4>
- [13] C. Tan, H. Zhao, and H. Ding, "Non-redundant inertial parameters determination for dynamic identification of branched articulated robots," *Industrial Robot: the international journal of robotics research and application*, vol. 49, no. 6, pp. 1229–1241, Sep. 2022. [Online]. Available: <https://www.emerald.com/insight/content/doi/10.1108/IR-12-2021-0296/full/html>
- [14] A. M. Shafei and H. R. Shafei, "Dynamic modeling of tree-type robotic systems by combining  $3 \times 3$  rotation and  $4 \times 4$  transformation matrices," *Multibody System Dynamics*, vol. 44, no. 4, pp. 367–395, Dec. 2018. [Online]. Available: <http://link.springer.com/10.1007/s11044-018-09642-4>
- [15] M. Ahmadizadeh, A. Shafei, and M. Fooladi, "Dynamic analysis of multiple inclined and frictional impact-contacts in multi-branch robotic systems," *Applied Mathematical Modelling*, vol. 91, pp. 24–42, Mar. 2021. [Online]. Available: <https://linkinghub.elsevier.com/retrieve/pii/S0307904X20305370>
- [16] K. Wang, P. Yin, H. Yang, and L. Wang, "Motion planning of rigid chain for rigid-flexible coupled robot," *International Journal of Advanced Robotic Systems*, vol. 15, no. 3, p. 172988141877281, May 2018. [Online]. Available: <http://journals.sagepub.com/doi/10.1177/1729881418772815>
- [17] P. E. Glick, I. Adibnazari, D. Drotman, D. Ruffatto Iii, and M. T. Tolley, "Branching Vine Robots for Unmapped Environments," *Frontiers in Robotics and AI*, vol. 9, p. 838913, Mar. 2022. [Online]. Available: <https://www.frontiersin.org/articles/10.3389/frobt.2022.838913/full>
- [18] X. Liu, B. You, R. Wang, Y. Zhao, C. Wei, and D. An, "Multi-Branch Cellular Space Robot Mechanism Design and Climbing Behavior Research," *Journal of Mechanisms and Robotics*, vol. 15, no. 5, p. 051016, Oct. 2023. [Online]. Available: <https://asmedigitalcollection.asme.org/mechanismsrobotics/article/15/5/051016/1155866/Multi-Branch-Cellular-Space-Robot-Mechanism-Design>
- [19] K. Kotay, D. Rus, M. Vona, and C. McGray, "The self-reconfiguring robotic molecule," in *Proceedings. 1998 IEEE International Conference on Robotics and Automation (Cat. No.98CH36146)*, vol. 1. IEEE, 1998, pp. 424–431. [Online]. Available: <http://ieeexplore.ieee.org/document/676452/>
- [20] J. Neubert and H. Lipson, "Soldercubes: A self-soldering self-reconfiguring modular robot system," *Autonomous Robots*, vol. 40, no. 1, pp. 139–158, Jan. 2016. [Online]. Available: <http://link.springer.com/10.1007/s10514-015-9441-4>
- [21] C. Unsal and P. Khosla, "Mechatronic design of a modular self-reconfiguring robotic system," in *Proceedings 2000 ICRA. Millennium Conference. IEEE International Conference on Robotics and Automation. Symposia Proceedings*, vol. 2. IEEE, 2000, pp. 1742–1747. [Online]. Available: <http://ieeexplore.ieee.org/document/844847/>
- [22] G. Andrews and H. Kesavan, "The vector-network model: A new approach to vector dynamics," *Mechanism and Machine Theory*, vol. 10, no. 1, pp. 57–75, Feb. 1975. [Online]. Available: <https://linkinghub.elsevier.com/retrieve/pii/0094114X75900579>
- [23] J. Chou, K. Singhal, and H. Kesavan, "Multi-body systems with open chains: Graph-theoretic models," *Mechanism and Machine Theory*, vol. 21, no. 3, pp. 273–284, Jan. 1986. [Online]. Available: <https://linkinghub.elsevier.com/retrieve/pii/0094114X86901035>
- [24] P. N. Sheth and J. J. Uicker, "IMP (Integrated Mechanisms Program), A Computer-Aided Design Analysis System for Mechanisms and Linkage," *Journal of Engineering for Industry*, vol. 94, no. 2, pp. 454–464, May 1972. [Online]. Available: <https://asmedigitalcollection.asme.org/manufacturingscience/article/94/2/454/427880/IMP-Integrated-Mechanisms-Program-A-ComputerAided>
- [25] G. C. Andrews, M. J. Richard, and R. J. Anderson, "A general vector-network formulation for dynamic systems with kinematic constraints," *Mechanism and Machine Theory*, vol. 23, no. 3, pp. 243–256, Jan. 1988. [Online]. Available: <https://linkinghub.elsevier.com/retrieve/pii/0094114X88901097>
- [26] G. Baciuc, J. Chou, and H. Kesavan, "Constrained multibody systems: Graph-theoretic Newton-Euler formulation," *IEEE Transactions on Systems, Man, and Cybernetics*, vol. 20, no. 5, pp. 1025–1048, 1990. [Online]. Available: <http://ieeexplore.ieee.org/document/59967/>
- [27] J. J. McPhee, "On the use of linear graph theory in multibody system dynamics," *Nonlinear Dynamics*, vol. 9, no. 1-2, pp. 73–90, Feb. 1996. [Online]. Available: <http://link.springer.com/10.1007/BF01833294>
- [28] —, "Automatic generation of motion equations for planar mechanical systems using the new set of "branch coordinates"," *Mechanism and Machine Theory*, vol. 33, no. 6, pp. 805–823, Aug. 1998. [Online]. Available: <https://linkinghub.elsevier.com/retrieve/pii/S0094114X97000554>
- [29] A. Reungwetwattana and S. Toyama, "An Efficient Dynamic Formulation for Multibody Systems," *Multibody System Dynamics*, vol. 6, no. 3, pp. 267–289, 2001.
- [30] J. C. K. Chou, H. K. Kesavan, and K. Singhal, "A Systems Approach to Three-Dimensional Multibody Systems Using Graph-Theoretic Models," *IEEE Transactions on Systems, Man, and Cybernetics*, vol. 16, no. 2, pp. 219–230, 1986. [Online]. Available: <http://ieeexplore.ieee.org/document/4308942/>
- [31] R. S. Hwang and E. J. Haug, "Topological Analysis of Multibody Systems for Recursive Dynamics Formulations," *Mechanics of Structures*

- and Machines, vol. 17, no. 2, pp. 239–258, Jun. 1989. [Online]. Available: <http://www.tandfonline.com/doi/abs/10.1080/15397738909412818>
- [32] M. Althoff, A. Giusti, S. B. Liu, and A. Pereira, “Effortless creation of safe robots from modules through self-programming and self-verification,” *Science Robotics*, vol. 4, no. 31, p. eaaw1924, Jun. 2019. [Online]. Available: <https://www.science.org/doi/10.1126/scirobotics.aaw1924>
- [33] A. Jain, “Multibody graph transformations and analysis,” *Nonlinear Dynamics*, vol. 67, no. 4, pp. 2779–2797, Mar. 2012. [Online]. Available: <http://link.springer.com/10.1007/s11071-011-0188-y>
- [34] J. McPhee, C. Schmitke, and S. Redmond, “Dynamic Modelling of Mechatronic Multibody Systems With Symbolic Computing and Linear Graph Theory,” *Mathematical and Computer Modelling of Dynamical Systems*, vol. 10, no. 1, pp. 1–23, Mar. 2004. [Online]. Available: <http://www.tandfonline.com/doi/abs/10.1080/13873950412331318044>
- [35] R. M. M. Orsino and T. A. Hess-Coelho, “A contribution on the modular modelling of multibody systems,” *Proceedings of the Royal Society A: Mathematical, Physical and Engineering Sciences*, vol. 471, no. 2183, p. 20150080, Nov. 2015. [Online]. Available: <https://royalsocietypublishing.org/doi/10.1098/rspa.2015.0080>
- [36] R. M. M. Orsino, “Recursive modular modelling methodology for lumped-parameter dynamic systems,” *Proceedings of the Royal Society A: Mathematical, Physical and Engineering Sciences*, vol. 473, no. 2204, p. 20160891, 2017. [Online]. Available: <https://royalsocietypublishing.org/doi/10.1098/rspa.2016.0891>
- [37] S. Kumar, K. A. V. Szadkowski, A. Mueller, and F. Kirchner, “An Analytical and Modular Software Workbench for Solving Kinematics and Dynamics of Series-Parallel Hybrid Robots,” *Journal of Mechanisms and Robotics*, vol. 12, no. 2, p. 021114, Apr. 2020. [Online]. Available: <https://asmedigitalcollection.asme.org/mechanismsrobotics/article/doi/10.1115/1.4045941/1072471/An-Analytical-and-Modular-Software-Workbench-for>
- [38] T. A. Hess-Coelho, R. M. M. Orsino, and F. Malvezzi, “Modular modelling methodology applied to the dynamic analysis of parallel mechanisms,” *Mechanism and Machine Theory*, vol. 161, p. 104332, Jul. 2021. [Online]. Available: <https://doi.org/10.1016/j.mechmachtheory.2021.104332>
- [39] A. Müller, “A note on the motion representation and configuration update in time stepping schemes for the constrained rigid body,” *BIT Numerical Mathematics*, vol. 56, no. 3, pp. 995–1015, Sep. 2016. [Online]. Available: <http://link.springer.com/10.1007/s10543-015-0580-y>
- [40] J. Yang, H. Peng, W. Zhou, J. Zhang, and Z. Wu, “A modular approach for dynamic modeling of multisegment continuum robots,” *Mechanism and Machine Theory*, vol. 165, p. 104429, Nov. 2021. [Online]. Available: <https://linkinghub.elsevier.com/retrieve/pii/S0094114X21001877>
- [41] J. Y. S. Luh, M. W. Walker, and R. P. C. Paul, “On-Line Computational Scheme for Mechanical Manipulators,” *Journal of Dynamic Systems, Measurement, and Control*, vol. 102, no. 2, pp. 69–76, Jun. 1980. [Online]. Available: <https://asmedigitalcollection.asme.org/dynamicsystems/article/102/2/69/399118/On-Line-Computational-Scheme-for-Mechanical>
- [42] B. V. Adorno, “Robot Kinematic Modeling and Control Based on Dual Quaternion Algebra – Part I: Fundamentals,” Tech. Rep., 2017. [Online]. Available: <https://hal.archives-ouvertes.fr/hal-01478225v1>
- [43] S. M. LaValle, *Planning Algorithms*. Cambridge: Cambridge University Press, 2006. [Online]. Available: <http://planning.cs.uiuc.edu/>
- [44] J. Funda, R. H. Taylor, and R. P. Paul, “On Homogeneous Transforms, Quaternions, and Computational Efficiency,” *IEEE Transactions on Robotics and Automation*, vol. 6, no. 3, pp. 382–388, 1990.
- [45] N. A. Aspragathos and J. K. Dimitros, “A comparative study of three methods for robot kinematics,” *IEEE Transactions on Systems, Man, and Cybernetics, Part B: Cybernetics*, vol. 28, no. 2, pp. 135–145, 1998.
- [46] F. F. A. Silva, J. J. Quiroz-Omaña, and B. V. Adorno, “Dynamics of Mobile Manipulators using Dual Quaternion Algebra,” *Journal of Mechanisms and Robotics*, vol. 14, no. 6, p. 11, Jan. 2022. [Online]. Available: <https://arxiv.org/abs/2007.08444>
- [47] T. H. Cormen, C. E. Leiserson, R. L. Rivest, and C. Stein, *Introduction to Algorithms*. London: The MIT Press, 2009.
- [48] H. Gazit and G. L. Miller, “An improved parallel algorithm that computes the BFS numbering of a directed graph,” *Information Processing Letters*, vol. 28, no. 2, pp. 61–65, Jun. 1988.
- [49] C. E. Leiserson and T. B. Schardl, “A work-efficient parallel breadth-first search algorithm (or how to cope with the nondeterminism of reducers),” in *Proceedings of the Twenty-Second Annual ACM Symposium on Parallelism in Algorithms and Architectures*. Thira Santorini Greece: ACM, Jun. 2010, pp. 303–314.
- [50] A. Buluç and K. Madduri, “Parallel breadth-first search on distributed memory systems,” in *Proceedings of 2011 International Conference for High Performance Computing, Networking, Storage and Analysis*. Seattle Washington: ACM, Nov. 2011, pp. 1–12.
- [51] F. F. A. Silva and B. V. Adorno, “Whole-body Control of a Mobile Manipulator Using Feedback Linearization and Dual Quaternion Algebra,” *Journal of Intelligent & Robotic Systems*, vol. 91, no. 2, pp. 249–262, Aug. 2018. [Online]. Available: <https://link.springer.com/article/10.1007/s10846-017-0686-3>
- [52] E. Rohmer, S. P. N. Singh, and M. Freese, “V-REP: A versatile and scalable robot simulation framework,” in *2013 IEEE/RSJ International Conference on Intelligent Robots and Systems*. IEEE, Nov. 2013, pp. 1321–1326. [Online]. Available: <http://ieeexplore.ieee.org/document/6696520/>
- [53] E. Todorov, T. Erez, and Y. Tassa, “MuJoCo: A physics engine for model-based control,” in *2012 IEEE/RSJ International Conference on Intelligent Robots and Systems*. Vilamoura-Algarve, Portugal: IEEE, Oct. 2012, pp. 5026–5033. [Online]. Available: <http://ieeexplore.ieee.org/document/6386109/>
- [54] B. V. Adorno and M. Marques Marinho, “DQ Robotics: A Library for Robot Modeling and Control,” *IEEE Robotics & Automation Magazine*, vol. 28, no. 3, pp. 102–116, Sep. 2021. [Online]. Available: <https://ieeexplore.ieee.org/document/9136790/>
- [55] A. Gilat and V. Subramaniam, *Numerical Methods for Engineers and Scientists: An Introduction with Applications Using MATLAB*, L. Ratts and H. Ellis, Eds. Hoboken, USA: John Wiley & Sons, 2014.
- [56] A. Ferrari, A. G. Cutti, and A. Cappello, “A new formulation of the coefficient of multiple correlation to assess the similarity of waveforms measured synchronously by different motion analysis protocols,” *Gait & Posture*, vol. 31, no. 4, pp. 540–542, Apr. 2010. [Online]. Available: <http://dx.doi.org/10.1016/j.gaitpost.2010.02.009>
- [57] K. Bouyarmane, K. Chappellet, J. Vaillant, and A. Kheddar, “Quadratic Programming for Multirobot and Task-Space Force Control,” *IEEE Transactions on Robotics*, vol. 35, no. 1, pp. 64–77, Feb. 2019. [Online]. Available: <https://ieeexplore.ieee.org/document/8528498/>
- [58] B. V. Adorno, “Two-arm Manipulation: From Manipulators to Enhanced Human-Robot Collaboration [Contribution à la manipulation à deux bras : Des manipulateurs à la collaboration homme-robot],” Ph.D. dissertation, Université de Montpellier, 2011.